

Effective viscosity of dense colloidal crystals

J. M. A. Hofman, H. J. H. Clercx, and P. P. J. M. Schram

Department of Physics, Eindhoven University of Technology, P.O. Box 513, 5600 MB Eindhoven, The Netherlands

(Received 3 August 1999; revised manuscript received 22 June 2000)

An exact scheme is presented to determine the effective viscosity tensor for periodic arrays of hard spherical particles suspended in a Newtonian fluid. In the highly symmetric case of cubic lattices this tensor is characterized by only two parameters. These parameters are calculated numerically for the three cubic lattice types and for the whole range of volume fractions. The correctness of the present method and its numerical implementation is confirmed by a comparison with the numerical and analytical results known from the literature. Some regular terms are determined that enter singular perturbation expansions suitable for high concentrations. Previous results for these terms are shown to be highly inaccurate. The modified expansions approach the exact numerical results over a range of densities extending to relatively low concentrations. The effective viscosity is examined for simple tetragonal (st) lattices and the results for various structures of the st type can be qualitatively understood on the basis of the motion of the spheres in response to the ambient shear flow. The angular velocity of the spheres—relative to the shear flow—is shown to be nonzero for certain orientations of the st lattice with respect to the shear flow, in contrast to what has been known for cubic arrays. Finite viscosities are found in most cases where the particles are in contact as they are allowed to move in either rigid planar or linelike structures, or they can perform a smooth rolling motion. The only occurrence where the viscosity diverges for a st structure, or equally any other Bravais lattice, is for the case of close packing. Moreover, the concentration-dependent shear viscosity is determined for a variety of microstructures and the results are compared with recent data obtained from experiments on ordered hard-sphere suspensions.

PACS number(s): 83.70.Hq, 83.50.-v, 47.15.Gf, 47.35.+i

I. INTRODUCTION

In the past few decades ordered suspensions of mesoscopic particles known as colloidal crystals have gained considerable interest as model systems to study a wide variety of physical phenomena, ranging from crystallization and melting [1–5] and Brownian motion [6–12] to sedimentation [13,14] and optical and acoustic band gaps [15–17]. Long range order in colloidal crystals can be due to various interactions between the suspended particles, viz., electrostatic [6,7,18], magnetostatic [19,20], hydrodynamic [21,22], or depletion (entropic) interactions [1,3,4], and in many cases combinations of these effects, depending on the various characteristics of both particles and solvent fluid. These interactions are also subject to intensive investigation, generally in close connection with the above mentioned phenomena [6,7,2,23,24,12]. In most experimental studies colloidal crystals consist of identical spherical particles, or well defined mixtures of spheres, which can be obtained through modern processing techniques. Sphere diameters are typically in the range of 10 nm to 10 μ m, which is large compared to atomic sizes in “normal” crystals. In fact, by virtue of thermodynamic analogy, colloidal crystals are frequently used to obtain insight into fundamental processes of atomic crystals, because these systems provide easily accessible time and length scales and since interactions can often be manipulated [5,25].

What makes colloidal crystals quite different from their atomic counterparts, however, is the presence of fluid surrounding the particles. Thus, moving particles can interchange momentum through the mediation of the fluid. Even if a certain particle is not moving at all (relative to an ambient flow) its mere presence will generally disturb the flow,

and thereby forces, torques, and higher moments of the force distribution (e.g., stresslets) are exerted on other particles. In order to determine such *hydrodynamic interactions* quantitatively, it is necessary to study particle motions as well as the flow of the solvent fluid, in detail. In a previous article [26], hereinafter referred to as I, we presented a rigorous method to study hydrodynamic interactions in concentrated colloidal crystals based on a formalism introduced by Clercx [27–29]. Fluid motion is described by the time-independent Stokes equations, which have been successfully used in many studies on low-Reynolds-number flow in suspensions of mesoscopic particles (see, e.g., the books of Happel and Brenner [30] and of Kim and Karrila [31]). A short review of the literature on theoretical and numerical methods for calculating Stokes flow through spatially periodic arrays of particles can be found in article I.

The purpose of this article is to consider the relationship between the effective stress and the average rate of strain for a colloidal crystal subject to a linear ambient flow (a uniform shear flow). This effective stress is the stress that can be observed on a macroscopic scale, e.g., by means of a Couette apparatus. The colloidal crystal consists of periodic cells containing N rigid spherical particles immersed in a Newtonian fluid. The flow of the suspending fluid is governed by the Stokes equations. Additionally, it is assumed that the spheres are neutrally buoyant and free of forces and torques, which implies that they are carried along by the flow in such a way that their configuration is distorted. It is important to appreciate that the effective stress considered here is a quantity that depends on the macroscopic strain rate and the *instantaneous* particle configuration, as can be measured in an oscillating Couette flow with small deformation (small shear amplitude). Moreover, the frequency of the oscillations is

considered sufficiently high so that stress contributions due to Brownian motion can be neglected [32].

Under the conditions mentioned above, the (deviatoric part of the) effective stress is linearly related to the ambient rate of strain, which has been well known since the work of Batchelor [33]. The effective viscosity is defined to be the four-tensor in this relationship. With regard to the experimental situation, as mentioned above, this viscosity is often referred to as the *high-frequency effective viscosity*. As will be expounded below the viscosity can be calculated on the basis of the theory presented in article I, provided, obviously, that the configuration of particles is spatially periodic. This seems to preclude the possibility of studying finite crystal deformations. However, such a grave restriction is unnecessary since a periodic array of spheres in a uniform shear flow will remain periodic. A cubic lattice of spheres, for instance, may become triclinic, and this deformation can be determined from the grand mobility matrix, which gives the particle motions relative to a known ambient flow. For the special case of unidirectional flow, the lattice will become cubic again after a finite time, and this will be repeated periodically. In any case, the effective viscosity can be calculated for each lattice through which the configuration passes.

Experimental studies have pointed out that the effective viscosity of *random* suspensions shows a rapid increase as the volume fraction of solid particles, ϕ , is rising. The same qualitative behavior is found for cubic arrays of spheres, as was indicated by calculations of Kapral and Bedeaux [34], some 20 years ago. These authors concluded that the viscosity of regular arrays goes to infinity before the closest packing density is reached. For random suspensions a similar divergence of the viscosity below the random-close-packing concentration had previously been suggested by Mooney [35]. This singularity was supposed to be due to “self-crowding” of particles. Numerical computations and asymptotic expansions for cubic arrays by Nunan and Keller [36] have shown that Kapral and Bedeaux’s high-density results (for cubic lattices) are inaccurate. Moreover, these numerical computations clearly indicate a singularity which corresponds to the close packing concentration for each of the three cubic lattice types. In the past 50 years a variety of formulas have also been proposed to predict the viscosity of random suspensions over the entire range of volume fractions. For a short review thereof see the references mentioned in Ref. [37]. Whether these formulas are derived on firm theoretical or semiempirical grounds, they all include an algebraic singularity at a certain volume fraction (in a physical or an unphysical regime). Using these singular forms it is possible to describe the steep rise of the viscosity at high concentrations. It is not known to date, however, if there exists a critical concentration at which the viscosity should diverge for random suspensions. Clercx and Schram have recently presented an expression for the high-frequency effective viscosity for random suspensions, thereby taking into account hydrodynamic interactions between two particles only [37]. Their expression is in good agreement with experimental data and a reasonable correspondence is found with numerical data and numerical simulation results, up to concentrations of $\phi \approx 0.6$. This is remarkable, since for such high densities three- and more-particle hydrodynamic interactions are expected to become important. For random sus-

pensions the effects of multiparticle hydrodynamic interactions are extremely difficult to calculate in an exact way, *inter alia* due to the fact that these computations require evaluation of distribution functions for an arbitrarily large number of particles [37,38]. This difficulty is not encountered for the case of colloidal crystals where the microstructure is exactly known, not merely in a statistical sense. Moreover, due to the inherent periodicity of colloidal crystals, the problem of determining infinitely many-particle hydrodynamic interactions can be effectively reduced to that of a finite number of particles. This allows one to determine the effective viscosity for these systems with great accuracy, as will be shown in this paper by application of the theoretical approach presented in article I. Except for the fact that our results yield some general insight into the mechanisms that determine the effective viscosity in particle suspensions, the accurate data represent an invaluable reference against which the performance of numerical simulation schemes can be tested. These issues will be discussed below.

The organization of this article is as follows. Section II introduces the grand mobility matrix (as mentioned above) for an isolated group of spherical particles. The theoretical scheme for calculating the grand mobility matrix is expounded in Sec. III, which summarizes the analysis followed in article I and introduces some additional ingredients necessary for the determination of the effective viscosity. This culminates in a set of linear equations by which the mobility matrix can eventually be solved. In Sec. IV the set of linear equations is presented in a form that is suitable for calculation of the viscosity appropriate for the case of regular arrays. The procedure for performing these calculations is given in Sec. V. Explicit numerical results for the effective viscosity for cubic arrays are presented in Sec. VI. A detailed comparison with previous numerical data for a wide range of concentrations confirms the correctness of the present method and its numerical implementation. Using the numerical results for extremely high volume fractions, a correction is presented of the asymptotic formulas as found previously by Nunan and Keller. Next, Sec. VII is concerned with simple tetragonal arrays. The viscosity behavior for this type of structure is examined in connection with the motion of the particles in response to the ambient shear flow. Moreover, it is illustrated that finite viscosities are obtained for several configurations of touching particles. This finding also suggests the unlikelihood that the high-frequency viscosity of random hard-sphere suspensions should be singular before closest packing is reached. In Sec. VIII the viscosity results for a variety of regular arrays are compared to measurements of the viscosity of ordered suspensions, as reported recently by Gondret and Petit [21]. We end with a conclusion in Sec. IX.

II. THE GRAND MOBILITY MATRIX

The study of the effective viscosity is started by considering a system of N rigid spherical particles with radii a_n , $n \in \{1, 2, \dots, N\}$, immersed in an incompressible, unbounded fluid. Their centers have position vectors \mathbf{R}_n with respect to the origin O . It is assumed that the ambient velocity field $\mathbf{v}_a(\mathbf{r})$ of the fluid in the absence of particles is linear,

$$\mathbf{v}_a(\mathbf{r}) = \mathbf{V}_a + \boldsymbol{\omega}_a \times \mathbf{r} + \mathbf{g}_a \cdot \mathbf{r}, \quad (2.1)$$

with constant velocity \mathbf{V}_a , angular velocity $\boldsymbol{\omega}_a$, and traceless and symmetrical rate of strain tensor \mathbf{g}_a [39]. In the presence of particles $\mathbf{v}_a(\mathbf{r})$ is considered as the linear part of the total velocity field. The position vector \mathbf{r} is defined with respect to the origin O . Due to the ambient flow and possibly external forces the particles may have velocities \mathbf{U}_n and rotational velocities $\boldsymbol{\Omega}_n$. Even if a certain particle is not moving at all (relative to the ambient flow) its mere presence will generally disturb the flow, and thereby forces and torques are exerted on other particles. In order to determine such hydrodynamic interactions quantitatively, it is necessary to study particle motions as well as the flow of the solvent fluid, in detail. Under certain conditions, discussed in more detail in article I, the equations of motion of the continuous fluid are given by the Stokes equations, which express conservation of momentum and mass, as

$$\eta \nabla^2 \mathbf{v}(\mathbf{r}) - \nabla p(\mathbf{r}) = \mathbf{0}, \quad (2.2a)$$

$$\nabla \cdot \mathbf{v}(\mathbf{r}) = 0, \quad (2.2b)$$

with $\mathbf{v}(\mathbf{r})$ the fluid velocity at position \mathbf{r} and $p(\mathbf{r})$ the pressure [40]. The material property η is called the *dynamic viscosity*, and in most instances is simply referred to as the *viscosity*. One of the conditions for the validity of the Stokes equations is the smallness of the Reynolds number corresponding to the disturbance of fluid motion caused by the presence of a representative spherical particle with radius a , in the ambient flow. This Reynolds number is given by $Re = \dot{\gamma} a^2 / \nu$, where $\dot{\gamma}$ is a representative magnitude of the ambient rate of strain and $\nu = \eta / \rho$ is the kinematic viscosity of the suspending fluid. In addition to satisfying the Stokes equations (2.2) outside the N spheres, the flow is assumed to obey *stick* boundary conditions on the surfaces of all particles. This means for $\mathbf{v}(\mathbf{r})$ at the surface S_n of particle n :

$$\mathbf{v}(\mathbf{r}) = \mathbf{U}_n + \boldsymbol{\Omega}_n \times (\mathbf{r} - \mathbf{R}_n) \quad \text{with } \mathbf{r} \in S_n. \quad (2.3)$$

After calculation of $\mathbf{v}(\mathbf{r})$ and $p(\mathbf{r})$ as expounded in the following section, the pressure tensor $\boldsymbol{\Pi}(\mathbf{r})$ can be determined, defined by

$$\boldsymbol{\Pi}(\mathbf{r}) = p(\mathbf{r}) \mathbf{1} - \eta [\nabla \mathbf{v}(\mathbf{r}) + [\nabla \mathbf{v}(\mathbf{r})]^T]. \quad (2.4)$$

The pressure tensor is used to calculate the force \mathbf{F}_n , the torque \mathbf{T}_n and the stresslet \mathbf{S}_n exerted by the fluid on particle n . The force and torque satisfy

$$\mathbf{F}_n = - \int_{S_n} \boldsymbol{\Pi}(\mathbf{r}) \cdot \mathbf{n} dA, \quad (2.5a)$$

$$\mathbf{T}_n = - \int_{S_n} \mathbf{r} \times \boldsymbol{\Pi}(\mathbf{r}) \cdot \mathbf{n} dA, \quad (2.5b)$$

where \mathbf{n} is the unit vector normal to the surface element dA and directed into the fluid. The stresslet \mathbf{S}_n is the traceless and symmetrical part of the first moment of the force distribution integrated over the surface of particle n ,

$$\mathbf{S}_n = - \int_{S_n} \overline{\mathbf{r} \boldsymbol{\Pi}(\mathbf{r})} \cdot \mathbf{n} dA, \quad (2.6)$$

where $\overline{\mathbf{r} \boldsymbol{\Pi}(\mathbf{r}) \cdot \mathbf{n}}$ denotes the traceless and symmetrical part of the dyad $\mathbf{r} \boldsymbol{\Pi}(\mathbf{r}) \cdot \mathbf{n}$. In order to define the grand mobility matrix it is useful to introduce the N -particle velocity and rotational velocity vectors

$$\mathbf{U} = (\mathbf{U}_1, \dots, \mathbf{U}_N), \quad \boldsymbol{\Omega} = (\boldsymbol{\Omega}_1, \dots, \boldsymbol{\Omega}_N) \quad (2.7)$$

and similar notations for the quantities related to the ambient velocity field,

$$\mathbf{U}_a = (\mathbf{U}_{a1}, \dots, \mathbf{U}_{aN}), \quad (2.8a)$$

$$\boldsymbol{\Omega}_a = (\boldsymbol{\omega}_{a1}, \dots, \boldsymbol{\omega}_{aN}), \quad (2.8b)$$

$$\mathbf{G}_a = (\mathbf{g}_{a1}, \dots, \mathbf{g}_{aN}). \quad (2.8c)$$

Here

$$\mathbf{U}_{an} = \mathbf{v}_a(\mathbf{R}_n) = \mathbf{V}_a + \boldsymbol{\omega}_a \times \mathbf{R}_n + \mathbf{g}_a \cdot \mathbf{R}_n, \quad (2.9a)$$

$$\boldsymbol{\omega}_{an} = \boldsymbol{\omega}_a, \quad (2.9b)$$

$$\mathbf{g}_{an} = \mathbf{g}_a. \quad (2.9c)$$

Analogous to the kinematic quantities in Eq. (2.7), the forces, torques, and stresslets can be combined into the arrays

$$\mathbf{F} = (\mathbf{F}_1, \dots, \mathbf{F}_N), \quad (2.10a)$$

$$\mathbf{T} = (\mathbf{T}_1, \dots, \mathbf{T}_N), \quad (2.10b)$$

$$\mathbf{S} = (\mathbf{S}_1, \dots, \mathbf{S}_N). \quad (2.10c)$$

Because of the linearity of the ambient flow (2.1), the Stokes equations (2.2), and the boundary conditions (2.3), there exists a linear relationship between the N -particle velocity difference $\mathbf{U} - \mathbf{U}_a$ and the given quantities \mathbf{F} , \mathbf{T} , and \mathbf{G}_a . Analogously, the rotational velocity difference $\boldsymbol{\Omega} - \boldsymbol{\Omega}_a$ and the stresslet \mathbf{S} depend linearly on \mathbf{F} , \mathbf{T} , and \mathbf{G}_a . These relations can be expressed in condensed form as

$$\begin{pmatrix} \mathbf{U} - \mathbf{U}_a \\ \boldsymbol{\Omega} - \boldsymbol{\Omega}_a \\ -\mathbf{S} \end{pmatrix} = - \begin{pmatrix} \boldsymbol{\mu}^{tt} & \boldsymbol{\mu}^{tr} & \boldsymbol{\mu}^{td} \\ \boldsymbol{\mu}^{rt} & \boldsymbol{\mu}^{rr} & \boldsymbol{\mu}^{rd} \\ \boldsymbol{\mu}^{dt} & \boldsymbol{\mu}^{dr} & \boldsymbol{\mu}^{dd} \end{pmatrix} \cdot \begin{pmatrix} \mathbf{F} \\ \mathbf{T} \\ \mathbf{G}_a \end{pmatrix}. \quad (2.11)$$

The submatrices $\boldsymbol{\mu}^{tt}$, etc., are composed of mobility tensors $\boldsymbol{\mu}_{ij}^{tt}$, etc., where the superscripts t, r, and d refer to *translational*, *rotational*, and *dipole*, respectively. The dot in Eq. (2.11) stands for a contraction of tensors. It should be mentioned that in this notation for the mobility tensors no distinction has been made between tensors of different rank: e.g., $\boldsymbol{\mu}_{ij}^{tt}$ is a second rank tensor, $\boldsymbol{\mu}_{ij}^{dd}$ is a fourth rank tensor. The mobility tensors obey certain symmetry properties as a consequence of the Lorentz reciprocal theorem (see, e.g. Ref. [31]). For the tensor $\boldsymbol{\mu}^{dd}$ this yields

$$\boldsymbol{\mu}_{ij, \alpha\beta\gamma\delta}^{dd} = \boldsymbol{\mu}_{ji, \gamma\delta\alpha\beta}^{dd}, \quad (2.12)$$

which will be used hereafter.

III. THE SET OF LINEAR EQUATIONS

In order to calculate the grand mobility matrix for an ensemble of spherical particles it is necessary to solve the equations of motion of the continuous fluid (2.2) thereby satisfying the stick boundary condition (2.3) on each sphere. This subject has been discussed in the past by several authors and nowadays various methods are at our disposal to tackle the problem (see, e.g., Refs. [31,30] for a review). The set of basis solutions presented by Schmitz and Felderhof [41] provides an elegant and powerful method that has been applied successfully by Clercx and Schram in calculating the effects of two- and three-particle hydrodynamic interactions in suspensions [27,28,37]. This method relies on the linearity of the Stokes equations (2.2) to express the disturbance velocity field $\mathbf{v} - \mathbf{v}_a$ caused by the N moving spheres as a sum of velocity fields \mathbf{v}_n :

$$\mathbf{v}(\mathbf{r}) - \mathbf{v}_a(\mathbf{r}) = \sum_{n=1}^N \mathbf{v}_n(\mathbf{r} - \mathbf{R}_n), \quad (3.1)$$

where \mathbf{R}_n is the position vector of the n th sphere with respect to the origin O . All the N velocity fields can be expanded in terms of basis solutions of the Stokes equations $\mathbf{v}_{lm\alpha}$, $\mathbf{v}_{lm\beta}$, $\mathbf{v}_{lm\gamma}$ as follows:

$$\mathbf{v}_n(\mathbf{r}) = \sum_{l,m} [\alpha_{lm}^n \mathbf{v}_{lm\alpha}(\mathbf{r}) + \beta_{lm}^n \mathbf{v}_{lm\beta}(\mathbf{r}) + \gamma_{lm}^n \mathbf{v}_{lm\gamma}(\mathbf{r})], \quad (3.2)$$

with expansion coefficients $\alpha_{lm}^n, \beta_{lm}^n, \gamma_{lm}^n$ and $l \geq 1$, $-l \leq m \leq l$ in the summation. These basis solutions are, in spherical coordinates r, θ, ϕ ,

$$\mathbf{v}_{lm\alpha}(\mathbf{r}) = \frac{l}{(l+1)(2l+1)} r^{-(l+2)} \mathbf{B}_{lm}(\theta, \phi), \quad (3.3a)$$

$$\mathbf{v}_{lm\beta}(\mathbf{r}) = \frac{1}{l(l+1)} r^{-(l+1)} \mathbf{C}_{lm}(\theta, \phi), \quad (3.3b)$$

$$\mathbf{v}_{lm\gamma}(\mathbf{r}) = \frac{1}{(2l+1)} r^{-l} [(l+1) \mathbf{A}_{lm}(\theta, \phi) - \frac{1}{2} l(2l-1) \mathbf{B}_{lm}(\theta, \phi)], \quad (3.3c)$$

where the vector spherical harmonics \mathbf{A}_{lm} , \mathbf{B}_{lm} , and \mathbf{C}_{lm} can be expressed in terms of the spherical harmonics Y_{lm} and the unit vectors \mathbf{e}_r , \mathbf{e}_θ , \mathbf{e}_ϕ :

$$\begin{aligned} \mathbf{A}_{lm}(\theta, \phi) &= l Y_{lm}(\theta, \phi) \mathbf{e}_r + \frac{\partial Y_{lm}(\theta, \phi)}{\partial \theta} \mathbf{e}_\theta \\ &+ \frac{1}{\sin \theta} \frac{\partial Y_{lm}(\theta, \phi)}{\partial \phi} \mathbf{e}_\phi, \end{aligned} \quad (3.4a)$$

$$\mathbf{B}_{lm}(\theta, \phi) = \mathbf{A}_{lm}(\theta, \phi) - (2l+1) Y_{lm}(\theta, \phi) \mathbf{e}_r, \quad (3.4b)$$

$$\begin{aligned} \mathbf{C}_{lm}(\theta, \phi) &= \frac{1}{\sin \theta} \frac{\partial Y_{lm}(\theta, \phi)}{\partial \phi} \mathbf{e}_\theta - \frac{\partial Y_{lm}(\theta, \phi)}{\partial \theta} \mathbf{e}_\phi \\ &= \mathbf{A}_{lm}(\theta, \phi) \times \mathbf{e}_r. \end{aligned} \quad (3.4c)$$

For completeness it should be noted that we use the following convention for the spherical harmonics in connection with the associated Legendre functions P_l^m (see, e.g., Ref. [42]):

$$Y_{lm}(\theta, \phi) = \frac{(-1)^m}{n_{lm}} P_l^m(\cos \theta) e^{im\phi} \quad (3.5)$$

for $m \geq 0$, with the normalization constants

$$n_{lm} = \left[\frac{4\pi}{(2l+1)} \frac{(l+m)!}{(l-m)!} \right]^{1/2}. \quad (3.6)$$

The definition for $m < 0$ is given by

$$Y_{lm}^*(\theta, \phi) = (-1)^m Y_{l,-m}(\theta, \phi). \quad (3.7)$$

With regard to the decomposition of the velocity field in Eq. (3.1), it is evident that each of the N moving spheres also causes a pressure disturbance p_n . Analogously to \mathbf{v}_n in Eq. (3.2), these p_n can be expanded in terms of a set of basis functions as

$$p_n(\mathbf{r}) = \sum_{l,m} [\alpha_{lm}^n p_{lm\alpha}(\mathbf{r}) + \beta_{lm}^n p_{lm\beta}(\mathbf{r}) + \gamma_{lm}^n p_{lm\gamma}(\mathbf{r})]. \quad (3.8)$$

The pressure functions $p_{lm\alpha}$, $p_{lm\beta}$, $p_{lm\gamma}$ are chosen such that the Stokes equations

$$\eta \nabla^2 \mathbf{v}_{lm\sigma}(\mathbf{r}) - \nabla p_{lm\sigma}(\mathbf{r}) = \mathbf{0}, \quad \nabla \cdot \mathbf{v}_{lm\sigma} = 0 \quad (3.9)$$

are satisfied for all $l \geq 1$, $|m| \leq l$, and $\sigma \in \{\alpha, \beta, \gamma\}$. Considering Eqs. (3.3), (3.4), and (3.9) and the fact that the pressure is harmonic in consequence of the Stokes equations, the pressure functions are found to be

$$p_{lm\alpha}(\mathbf{r}) = 0, \quad (3.10a)$$

$$p_{lm\beta}(\mathbf{r}) = 0, \quad (3.10b)$$

$$p_{lm\gamma}(\mathbf{r}) = \eta l(2l-1) r^{-(l+1)} Y_{lm}(\theta, \phi). \quad (3.10c)$$

It is found convenient to introduce the new expansion coefficients

$$A_{lm}^{\pm} = \frac{(-1)^{l+m}}{n_{lm} a_n^{l+2}} [\alpha_{lm}^{\pm} (-1)^m \alpha_{l,-m}^n], \quad (3.11a)$$

$$B_{lm}^{\pm} = -i \frac{(-1)^{l+m}}{n_{lm} a_n^{l+1}} [\beta_{lm}^{\pm} (-1)^m \beta_{l,-m}^n], \quad (3.11b)$$

$$C_{lm}^{\pm} = \frac{(-1)^{l+m}}{n_{lm} a_n^l} [\gamma_{lm}^{\pm} (-1)^m \gamma_{l,-m}^n]. \quad (3.11c)$$

As can be seen from these definitions it is sufficient to use the coefficients A_{lm}^{n+} , B_{lm}^{n+} , C_{lm}^{n+} with $m \geq 0$ and the coefficients A_{lm}^{n-} , B_{lm}^{n-} , C_{lm}^{n-} with $m \geq 1$. Some of these coefficients determine the force \mathbf{F}_n , torque \mathbf{T}_n and stresslet \mathcal{S}_n exerted by the fluid on particle n . These relations follow by substitution of the expansions of the velocity and the pressure in the definitions (2.4)–(2.6); the calculations are de-

tailed in Ref. [27] for the force and torque, and in Ref. [37] for the stresslet. The resulting expressions are

$$\mathbf{F}_n = 2\pi\eta a_n(2C_{1,1}^{n+}\mathbf{e}_x + 2iC_{1,1}^{n-}\mathbf{e}_y + C_{1,0}^{n+}\mathbf{e}_z), \quad (3.12a)$$

$$\mathbf{T}_n = 2\pi i\eta a_n^2(2B_{1,1}^{n+}\mathbf{e}_x + 2iB_{1,1}^{n-}\mathbf{e}_y + B_{1,0}^{n+}\mathbf{e}_z), \quad (3.12b)$$

$$\mathbf{S}_n = -\frac{1}{2}\eta a_n^2\left(\sum_{m=0}^2\chi_m C_{2m}^{n+}\boldsymbol{\tau}_m + \sum_{m=1}^2\chi_{-m} C_{2m}^{n-}\boldsymbol{\tau}_{-m}\right). \quad (3.12c)$$

Here the constant factors χ_q for $q \in \{-2, -1, 0, 1, 2\}$ are given by

$$\chi_0 = -\frac{4}{3}\sqrt{6}\pi, \quad \chi_1 = 8\sqrt{2}\pi, \quad \chi_{-1} = 8\sqrt{2}\pi i, \quad (3.13a)$$

$$\chi_2 = 16\sqrt{2}\pi, \quad \chi_{-2} = 16\sqrt{2}\pi i. \quad (3.13b)$$

The five tensors $\boldsymbol{\tau}_q$ form a basis for the traceless and symmetrical two-tensors, defined by

$$\begin{aligned} \boldsymbol{\tau}_0 &= \frac{1}{6}\sqrt{6}(\mathbf{e}_x\mathbf{e}_x + \mathbf{e}_y\mathbf{e}_y - 2\mathbf{e}_z\mathbf{e}_z), \\ \boldsymbol{\tau}_1 &= \frac{1}{2}\sqrt{2}(\mathbf{e}_x\mathbf{e}_z + \mathbf{e}_z\mathbf{e}_x), \\ \boldsymbol{\tau}_{-1} &= \frac{1}{2}\sqrt{2}(\mathbf{e}_y\mathbf{e}_z + \mathbf{e}_z\mathbf{e}_y), \\ \boldsymbol{\tau}_2 &= \frac{1}{2}\sqrt{2}(\mathbf{e}_x\mathbf{e}_x - \mathbf{e}_y\mathbf{e}_y), \\ \boldsymbol{\tau}_{-2} &= \frac{1}{2}\sqrt{2}(\mathbf{e}_x\mathbf{e}_y + \mathbf{e}_y\mathbf{e}_x). \end{aligned} \quad (3.14)$$

For instance, the traceless and symmetric strain rate \mathbf{g}_a can be expanded in terms of the above basis tensors as

$$\mathbf{g}_a = \sum_{q=-2}^2 \tilde{A}_q \boldsymbol{\tau}_q, \quad (3.15)$$

introducing the expansion coefficients \tilde{A}_q . Moreover, it is worthwhile to mention that the above basis is orthonormal:

$$\boldsymbol{\tau}_q : \boldsymbol{\tau}_{q'} = \delta_{qq'}. \quad (3.16)$$

This orthonormality will turn out to be convenient in future applications.

The unknown coefficients in Eq. (3.11) can be determined by application of the stick boundary conditions on the sphere surfaces. Following the procedure outlined in article I this eventually leads to a set of linear equations relating the unknown coefficients to the coefficients \tilde{A}_q that determine the strain rate \mathbf{g}_a , and the components of the particle velocities relative to the ambient flow $\tilde{\mathbf{U}}_n$ and $\tilde{\boldsymbol{\Omega}}_n$. These relative velocities are defined by

$$\tilde{\mathbf{U}}_n = \mathbf{U}_n - \mathbf{U}_{an}, \quad \tilde{\boldsymbol{\Omega}}_n = \boldsymbol{\Omega}_n - \boldsymbol{\omega}_a, \quad (3.17)$$

with \mathbf{U}_{an} as given by Eq. (2.9). On the basis of the above mentioned linear equations it is possible to determine the components of the grand mobility matrix defined by Eq. (2.11). It is noted that the set of equations comprises an infinite number of equations for an infinite number of coefficients $A_{lm}^{n\pm}$, $B_{lm}^{n\pm}$, and $C_{lm}^{n\pm}$ because the index l is un-

bounded. In order to solve the set of linear equations we define an upper limit L of this index, i.e., $l \leq L$, assuming all coefficients with $l > L$ to vanish. Thereby the number of equations is $3L(L+2)N$ with the same number of unknown coefficients. The choice of the truncation level L depends on various factors, e.g., the desired numerical accuracy. It is recalled that N denotes a (finite) number of particles, so that there is a finite number of equations that can be solved in a straightforward way.

IV. THE QUASI- N -PARTICLE APPROACH

Our aim is to determine the effective viscosity for the case of a regular array of spherical particles. The array consists of identical cells that contain N particles with radii a_n , $n \in \{0, 1, \dots, N-1\}$. It is assumed that this colloidal crystal is unbounded in all directions of three-dimensional space. The positions of the particles in the array, with respect to some origin \mathcal{O} , are specified by the vectors

$$\mathbf{R}_{\lambda n} = \mathbf{L}_\lambda + \mathbf{R}'_n. \quad (4.1)$$

Here \mathbf{R}'_n indicates the position of the n th particle relative to a lattice point, which is indicated by the lattice vector \mathbf{L}_λ . The lattice points form a regular array of points in space: a crystal lattice, or *Bravais lattice* as it is usually called.

The description of hydrodynamic interactions between particles in the array is based on the set of coupled linear equations discussed in the previous section. Direct application of these equations is not feasible however, because the number of equations is proportional to the number of interacting particles, which is assumed to be infinite in the present case. However, it is possible to exploit the translational invariance of the array, thereby obtaining a finite set of equations resembling that for an isolated system of N particles. This *quasi- N -particle approach*, expounded in detail in article I, relies on the fact that the mobility matrix for all (infinitely many) particles is solely determined by the geometry of the system: the periodic configuration of particle positions and particle sizes.

As shown in article I the quasi- N -particle approach enables one to study crystal waves, i.e., a lattice of particles executing translational and rotational motions that vary harmonically over the lattice. The set of linear equations derived in article I is also suitable to determine the effective viscosity, apart from a few minor modifications. These modifications concern the presence of the ambient flow (which was considered absent in article I) and the fact that the present problem yields a further simplification of the set of linear equations. In order to explain this simplification it is noted that the stresslets are linearly related to the strain rate, according to Eq. (2.11), and for forceless and torqueless particles these relations read

$$\mathbf{S}_n = \sum_j \boldsymbol{\mu}_{nj}^{\text{dd}} : \mathbf{g}_a. \quad (4.2)$$

Here summation is over all particles in the infinite array. By virtue of this equation, the translational symmetry of the lattice, and the fact that \mathbf{g}_a is constant, it follows that \mathbf{S}_n must be translationally symmetric also, i.e., the stresslet is the same for all particles at certain positions in the array that differ

exactly by one lattice vector. Thus, for cells containing N particles there are (at most) N different stresslets \mathbf{S}_n which can be written as

$$\mathbf{S}_n = \sum_{j=0}^{N-1} \hat{\boldsymbol{\mu}}_{nj}^{\text{dd}}(\mathbf{0}) : \mathbf{g}_a \quad (4.3)$$

for $n \in \{0, 1, \dots, N-1\}$. The Fourier transform used above is defined as

$$\hat{\boldsymbol{\mu}}_{nj}^{\text{dd}}(\mathbf{k}) = \sum_{\lambda} \boldsymbol{\mu}_{n,(\lambda j)}^{\text{dd}} e^{-i\mathbf{k} \cdot \mathbf{L}_{\lambda}}. \quad (4.4)$$

Here (λj) denotes the j th particle in the cell indicated by the lattice vector \mathbf{L}_{λ} and the summation runs over all lattice vectors of the infinite lattice. Notice that the Fourier transformed mobility tensor in Eq. (4.3) is evaluated at $\mathbf{k} = \mathbf{0}$. At this point it is found worthwhile to mention that the same translational symmetry applies to the relative velocities $\tilde{\mathbf{U}}_n$ and angular velocities $\tilde{\boldsymbol{\Omega}}_n$ defined by Eq. (3.17), and by analogy with Eq. (4.3) the N different $\tilde{\mathbf{U}}_n$ and $\tilde{\boldsymbol{\Omega}}_n$ are given by

$$\tilde{\mathbf{U}}_n = - \sum_{j=0}^{N-1} \hat{\boldsymbol{\mu}}_{nj}^{\text{td}}(\mathbf{0}) : \mathbf{g}_a, \quad \tilde{\boldsymbol{\Omega}}_n = - \sum_{j=0}^{N-1} \hat{\boldsymbol{\mu}}_{nj}^{\text{rd}}(\mathbf{0}) : \mathbf{g}_a. \quad (4.5)$$

Here $\hat{\boldsymbol{\mu}}_{nj}^{\text{td}}$ and $\hat{\boldsymbol{\mu}}_{nj}^{\text{rd}}$ are Fourier transformed mobility tensors defined analogously to $\hat{\boldsymbol{\mu}}_{nj}^{\text{dd}}$ in Eq. (4.4). The relations (4.5) will be useful later to determine particle motions in response to the ambient shear flow with strain rate tensor \mathbf{g}_a , whereas Eq. (4.3) can be used to determine the effective viscosity, as will be explained in the next section. Moreover, the translational invariance of the quantities $\tilde{\mathbf{U}}_n$ and $\tilde{\boldsymbol{\Omega}}_n$ yields a simplification of the set of linear equations, as mentioned before. By introducing new labels (λj) instead of n , with $j \in \{0, 1, \dots, N-1\}$ and λ labeling the cell indicated by the lattice vector \mathbf{L}_{λ} , this invariance can be expressed as

$$\tilde{\mathbf{U}}_{(\lambda j)} = \tilde{\mathbf{U}}_{(0j)}, \quad \tilde{\boldsymbol{\Omega}}_{(\lambda j)} = \tilde{\boldsymbol{\Omega}}_{(0j)}. \quad (4.6)$$

By virtue of these identities and the stick boundary conditions it can be straightforwardly shown (see Ref. [43]) that all expansion coefficients entering the set of linear equations are translationally symmetric, that is,

$$A_{lm}^{(\lambda j)\pm} = A_{lm}^{(0j)\pm}, \quad B_{lm}^{(\lambda j)\pm} = B_{lm}^{(0j)\pm}, \quad (4.7)$$

$$C_{lm}^{(\lambda j)\pm} = C_{lm}^{(0j)\pm}.$$

Following the procedure outlined in article I and taking notice of the translational symmetries expressed by Eqs. (4.6) and (4.7), a set of linear equations can be derived for the expansion coefficients in Eq. (4.7). These equations are

$$-\frac{3}{2} \delta_{p1} [\delta_{q1} \tilde{U}_{nx} + 2\delta_{q0} \tilde{U}_{nz}] - \frac{40\pi}{9} a_n \delta_{p2} \chi_q^{-1} \tilde{A}_q = C_{pq}^{n+} + \frac{2p+1}{p+1} \sum_{j=0}^{N-1} \sum_{l,m} \left[\frac{l}{(l+1)(2l+1)} X_{lm;pq}^{Rnj+}(\mathbf{0}) A_{lm}^{j+} \right. \\ \left. + \frac{il}{(l+1)(2l+1)} X_{lm;pq}^{Inj-}(\mathbf{0}) A_{lm}^{j-} + \frac{i}{pl(l+1)} Y_{lm;pq}^{Inj+}(\mathbf{0}) B_{lm}^{j+} \right. \\ \left. + \frac{1}{pl(l+1)} Y_{lm;pq}^{Rnj-}(\mathbf{0}) B_{lm}^{j-} + Z_{lm;pq}^{Rnj+}(\mathbf{0}) C_{lm}^{j+} + iZ_{lm;pq}^{Inj-}(\mathbf{0}) C_{lm}^{j-} \right], \quad (4.8)$$

$$\frac{3}{2} i \delta_{p1} \delta_{q1} \tilde{U}_{ny} - \frac{40\pi}{9} a_n \delta_{p2} \chi_q^{-1} \tilde{A}_{-q} = C_{pq}^{n-} + \frac{2p+1}{p+1} \sum_{j=0}^{N-1} \sum_{l,m} \left[\frac{il}{(l+1)(2l+1)} X_{lm;pq}^{Inj+}(\mathbf{0}) A_{lm}^{j+} + \frac{l}{(l+1)(2l+1)} X_{lm;pq}^{Rnj-}(\mathbf{0}) A_{lm}^{j-} \right. \\ \left. + \frac{1}{pl(l+1)} Y_{lm;pq}^{Rnj+}(\mathbf{0}) B_{lm}^{j+} + \frac{i}{pl(l+1)} Y_{lm;pq}^{Inj-}(\mathbf{0}) B_{lm}^{j-} + iZ_{lm;pq}^{Inj+}(\mathbf{0}) C_{lm}^{j+} + Z_{lm;pq}^{Rnj-}(\mathbf{0}) C_{lm}^{j-} \right], \quad (4.9)$$

$$A_{pq}^{n\pm} = \frac{1}{2}(p+1)(2p-1)C_{pq}^{n\pm} - \frac{1}{2p+3} \sum_{j=0}^{N-1} \sum_{l,m} l(2l-1) [X_{lm;pq}^{Rnj\pm}(\mathbf{0}) C_{lm}^{j\pm} + iX_{lm;pq}^{Inj\mp}(\mathbf{0}) C_{lm}^{j\mp}], \quad (4.10)$$

$$2ia_n \delta_{p1} [\delta_{q1} \tilde{\Omega}_{nx} + 2\delta_{q0} \tilde{\Omega}_{nz}] = B_{pq}^{n+} - \sum_{j=0}^{N-1} \sum_{l,m} \left[\frac{p}{l+1} X_{lm;pq}^{Rnj+}(\mathbf{0}) B_{lm}^{j+} + \frac{ip}{l+1} X_{lm;pq}^{Inj-}(\mathbf{0}) B_{lm}^{j-} \right. \\ \left. + i(2l-1) Y_{lm;pq}^{Inj+}(\mathbf{0}) C_{lm}^{j+} + (2l-1) Y_{lm;pq}^{Rnj-}(\mathbf{0}) C_{lm}^{j-} \right], \quad (4.11)$$

$$2a_n \delta_{p1} \delta_{q1} \tilde{\Omega}_{ny} = B_{pq}^{n-} - \sum_{j=0}^{N-1} \sum_{l,m} \left[\frac{ip}{l+1} X_{lm;pq}^{Inj+}(\mathbf{0}) B_{lm}^{j+} + \frac{p}{l+1} X_{lm;pq}^{Rnj-}(\mathbf{0}) B_{lm}^{j-} + (2l-1) Y_{lm;pq}^{Rnj+}(\mathbf{0}) C_{lm}^{j+} + i(2l-1) Y_{lm;pq}^{Inj-}(\mathbf{0}) C_{lm}^{j-} \right], \quad (4.12)$$

with $l \geq 1$, $0 \leq m \leq l$ in the summations. Moreover $p \geq 1$, $0 \leq q \leq p$, and $n \in \{0, 1, \dots, N-1\}$. Notice that the functions $X_{lm;pq}^{Rnj\pm}(\mathbf{k})$, $X_{lm;pq}^{Inj\pm}(\mathbf{k})$, $Y_{lm;pq}^{Rnj\pm}(\mathbf{k})$, $Y_{lm;pq}^{Inj\pm}(\mathbf{k})$, $Z_{lm;pq}^{Rnj\pm}(\mathbf{k})$, and $Z_{lm;pq}^{Inj\pm}(\mathbf{k})$, as defined in article I, are evaluated at $\mathbf{k}=\mathbf{0}$.

For a given truncation level L Eqs. (4.8)–(4.12) represent $3L(L+2)N$ equations, with the same number of coefficients $A_{lm}^{n\pm}$, $B_{lm}^{n\pm}$, and $C_{lm}^{n\pm}$. The number of equations can be reduced by expressing the coefficients $A_{lm}^{n\pm}$ in terms of $C_{lm}^{n\pm}$, through Eq. (4.10), getting $2L(L+2)N$ equations for the coefficients $B_{lm}^{n\pm}$ and $C_{lm}^{n\pm}$. At this point it should be noted that the equations for $p \geq 3$ are homogeneous, so that the coefficients with $l \geq 3$ can be expressed in terms of the coefficients with $l \leq 2$, exactly those coefficients determining the forces, torques, and stresslets according to Eq. (3.12) [44]. Due to vanishing forces and torques, this eventually leads to some linear relations between the five coefficients $C_{2m}^{n\pm}$ determining the stresslets and the five coefficients \tilde{A}_q that determine \mathbf{g}_a as given by Eq. (3.15). From these linear relations one can eventually obtain the effective viscosity, as discussed further in the next section. Additionally a set of linear relations is obtained between the coefficients \tilde{A}_q and the components of the relative velocities \tilde{U}_n and $\tilde{\Omega}_n$. In fact, these linear relations are precisely the mobility relations as given by Eqs. (4.3) and (4.5). It goes without saying that the procedure just described involves an enormous amount of effort, especially when we require an accurate solution of the mobilities for many-particle cells, that is, if L and N are large. Evidently, in these cases the help of the computer must be called upon. This numerical step comes down to solving a set of linear equations, for which efficient codes can be written.

It is important to note that some of the functions introduced in Eqs. (4.8)–(4.12) are singular at $\mathbf{k}=\mathbf{0}$. This holds in particular for the functions $Z_{2m;2q}^{Rnj\pm}(\mathbf{k})$ and $Z_{2m;2q}^{Inj\pm}(\mathbf{k})$ that enter the evaluation of the effective viscosity. These functions are found to have a discontinuity for vanishing wave vector. Moreover, if the relative velocities \tilde{U}_n are determined according to the relation (4.5) one is confronted with a divergence in the expression for $\hat{\mu}_{nj}^{\text{td}}(\mathbf{k})$ which behaves as k^{-1} . The various types of singularities are directly related to the long range dipolar interactions in the infinite regular array of spheres. In fact, for infinite arrays of particles, it is known that the disturbance velocity field can have a linear part. This point has been discussed by several authors in the context of polymer solutions [45], hard-sphere suspensions [46], and suspensions with periodic boundary conditions [47]. In this study we restrict ourselves to special cases where there is a unique way of taking the limit $\mathbf{k} \rightarrow \mathbf{0}$. This is the case, for example, when cubic, tetragonal, or hexagonal arrays are subject to certain shear flows, i.e., where the plane of shear coincides with a symmetry plane of the lattice. In these cases one can obtain convergent expressions for the relative velocities \tilde{U}_n if $\mathbf{k} \rightarrow \mathbf{0}$ is taken in the direction perpendicular to the plane of shear. Any other direction yields infinite velocities. The correctness of the proposed approach is supported by the analytical and numerical results presented in the following sections, which clearly show excellent agreement with data from the literature concerning this issue [34,36,48].

This procedure is followed in the rest of this article in order to determine the effective viscosity for a number of lattice types.

V. CALCULATION OF THE EFFECTIVE VISCOSITY

The effective stress σ_e for a suspension consisting of particles immersed in a fluid under slow flow conditions can be defined, according to Ref. [33], as the volume average of the local stress $\sigma(\mathbf{r})$ over a representative (macroscopic) region \mathcal{V} , with volume V , that contains both particles and fluid:

$$\sigma_e = \frac{1}{V} \int_{\mathcal{V}} \sigma(\mathbf{r}) d\mathbf{r}. \quad (5.1)$$

For colloidal crystals as described in the Introduction the region \mathcal{V} can be identified with a lattice cell containing N spheres. One can formally decompose \mathcal{V} into a region occupied by ambient fluid \mathcal{V}_f and the interior region of all N particles \mathcal{V}_p , thereby writing Eq. (5.1) in the form

$$\sigma_e = \frac{1}{V} \int_{\mathcal{V}_f} \sigma(\mathbf{r}) d\mathbf{r} + \frac{1}{V} \int_{\mathcal{V}_p} \sigma(\mathbf{r}) d\mathbf{r}. \quad (5.2)$$

As the suspending fluid is considered to be Newtonian the stress in \mathcal{V}_f is given by

$$\sigma(\mathbf{r}) = -\mathbf{\Pi}(\mathbf{r}), \quad (5.3)$$

where $\mathbf{\Pi}(\mathbf{r})$ is the pressure tensor defined by Eq. (2.4). Thus for rigid particles the first integral in Eq. (5.2) can be written (see, e.g., Ref. [31]) as

$$\frac{1}{V} \int_{\mathcal{V}_f} \sigma(\mathbf{r}) d\mathbf{r} = -p_e \mathbf{1} + \frac{2\eta}{V} \int_{\mathcal{V}} \overline{\nabla \mathbf{v}(\mathbf{r})} d\mathbf{r}. \quad (5.4)$$

Here the effective pressure p_e , defined by

$$p_e = \frac{1}{V} \int_{\mathcal{V}_f} p(\mathbf{r}) d\mathbf{r}, \quad (5.5)$$

provides the purely isotropic part of the stress, which is of no particular interest. The integral on the right-hand side of Eq. (5.4) (where the overbar denotes projection onto the symmetrical part) is proportional to the rate of strain averaged over \mathcal{V} (which contains both fluid and particles) [49]. Thus, by definition,

$$\frac{2\eta}{V} \int_{\mathcal{V}} \overline{\nabla \mathbf{v}(\mathbf{r})} d\mathbf{r} = 2\eta \mathbf{g}_a. \quad (5.6)$$

The contribution to the stress due to the presence of the particles, σ_p , is given by the second integral in Eq. (5.2). Following the analysis in Refs. [33,31] and restricting ourselves to forceless and torqueless particles, it is found that this particle stress is directly related to the stresslets S_i of the N spheres contained in a cell:

$$\sigma_p = \frac{1}{V} \sum_{i=0}^{N-1} S_i. \quad (5.7)$$

In order to define the effective viscosity it is found convenient to decompose the effective stress $\boldsymbol{\sigma}_e$ into the isotropic pressure term $-p_e \mathbb{1}$ and the deviatoric stress contribution $\boldsymbol{\sigma}_d$; thus

$$\boldsymbol{\sigma}_e = -p_e \mathbb{1} + \boldsymbol{\sigma}_d. \quad (5.8)$$

According to Eqs. (5.1), (5.2), (5.4), and (5.6) this deviatoric stress satisfies

$$\boldsymbol{\sigma}_d = 2\eta \mathbf{g}_a + \boldsymbol{\sigma}_p. \quad (5.9)$$

Combining this identity with Eqs. (4.3) and (5.7) yields

$$\boldsymbol{\sigma}_d = 2\eta \mathbf{g}_a + \frac{1}{V} \sum_{ij} \hat{\boldsymbol{\mu}}_{ij}^{\text{dd}}(\mathbf{0}) : \mathbf{g}_a. \quad (5.10)$$

This linear relation between the deviatoric stress and the rate of strain can be written in condensed form as

$$\boldsymbol{\sigma}_d = 2\boldsymbol{\eta}_e : \mathbf{g}_a. \quad (5.11)$$

The four-tensor $\boldsymbol{\eta}_e$ in this relationship will be called the effective viscosity. This effective viscosity can be determined by solving the components of the mobility tensors in Eq. (5.10) from the set of linear equations (4.8)–(4.12). In order to explain how this can be accomplished it is found convenient to introduce the four-tensor

$$\boldsymbol{\mu}^d = \frac{1}{2\eta V} \sum_{ij} \hat{\boldsymbol{\mu}}_{ij}^{\text{dd}}(\mathbf{0}). \quad (5.12)$$

This tensor satisfies certain symmetries which can be exploited to simplify the calculations. Combining Eqs. (5.12), (2.12), and (4.4) and using the symmetries of the crystal lattice (translational and inversion invariance), it follows that

$$\boldsymbol{\mu}_{\alpha\beta\gamma\delta}^d = \boldsymbol{\mu}_{\gamma\delta\alpha\beta}^d. \quad (5.13)$$

Furthermore, it is noted that the stresslets, the strain rate, and therefore also $\boldsymbol{\sigma}_d$ in Eq. (5.10) are symmetrical and traceless. As a direct inference from these properties, combined with the symmetry in Eq. (5.13), it follows that $\boldsymbol{\mu}^d$ is symmetric and traceless in both its first and second pair of indices:

$$\begin{aligned} \boldsymbol{\mu}_{\alpha\beta\gamma\delta}^d &= \boldsymbol{\mu}_{\beta\alpha\gamma\delta}^d, & \boldsymbol{\mu}_{\alpha\beta\gamma\delta}^d &= \boldsymbol{\mu}_{\alpha\beta\delta\gamma}^d, \\ \boldsymbol{\mu}_{\alpha\alpha\gamma\delta}^d &= 0, & \boldsymbol{\mu}_{\alpha\beta\gamma\gamma}^d &= 0. \end{aligned} \quad (5.14)$$

In the last two equations the trace is denoted by repeated indices, according to the Einstein summation convention. By virtue of the symmetry relations (5.13) and (5.14) it follows that $\boldsymbol{\mu}^d$ can be characterized by 25 numbers M_{mn} , for $m, n \in \{-2, -1, 0, 1, 2\}$, that are defined by

$$M_{mn} = \boldsymbol{\tau}_m : \boldsymbol{\mu}^d : \boldsymbol{\tau}_n. \quad (5.15)$$

The coefficients M_{mn} can be determined using the relations between the coefficients $C_{2q}^{i\pm}$ and $\tilde{A}_{\pm q}$, with $q \in \{0, 1, 2\}$. These relations are given by the set of linear equations (4.8)–(4.12). For that purpose it is recalled that the tensors $\boldsymbol{\tau}_m$, as

defined by Eq. (3.14), form a basis for the symmetrical and traceless two-tensors, so that the stresslets \mathcal{S}_i can be expanded as

$$\mathcal{S}_i = \sum_{m=-2}^2 \tilde{C}_m^i \boldsymbol{\tau}_m. \quad (5.16)$$

The coefficients \tilde{C}_m^i are related to the previously defined coefficients $C_{2q}^{i\pm}$ in Eq. (3.11) as

$$\tilde{C}_0^i = -\frac{3}{2} \eta a_i^2 \chi_0 C_{20}^{i+}, \quad \tilde{C}_{\pm q}^i = -\frac{3}{2} \eta a_i^2 \chi_{\pm q} C_{2q}^{i\pm}. \quad (5.17)$$

Here the subscripts $q \in \{1, 2\}$, and the constants χ_m for $m \in \{-2, -1, 0, 1, 2\}$ are defined by Eq. (3.13). As is inferred from Eq. (4.3) the coefficients \tilde{C}_m^i and \tilde{A}_n are linearly related, which can be expressed as

$$\tilde{C}_m^i = \sum_{n=-2}^2 D_{mn}^i \tilde{A}_n. \quad (5.18)$$

The proportionality constants D_{mn}^i are determined by the geometry of the array of spheres, as they are directly related to the mobilities in Eq. (4.3). In effect, it follows straightforwardly from Eqs. (4.3), (3.15), and (5.16) and the orthonormality relations for the tensors $\boldsymbol{\tau}_m$ in Eq. (3.16), that

$$D_{mn}^i = \boldsymbol{\tau}_m : \left[\sum_j \hat{\boldsymbol{\mu}}_{ij}^{\text{dd}}(\mathbf{0}) \right] : \boldsymbol{\tau}_n. \quad (5.19)$$

Combining this identity with the definitions (5.12) and (5.15) yields

$$M_{mn} = \frac{1}{2\eta V} \sum_i D_{mn}^i. \quad (5.20)$$

Moreover, by combination of Eqs. (3.15), (3.16), (5.11), (5.10), (5.12), and (5.15) it is found that the effective viscosity tensor has 25 components with respect to the basis of tensors $\boldsymbol{\tau}_m$ and these components are directly related to the matrix elements M_{mn} according to the identity

$$\boldsymbol{\tau}_m : \boldsymbol{\eta}_e : \boldsymbol{\tau}_n = \eta (\delta_{mn} + M_{mn}). \quad (5.21)$$

The 25 numbers M_{mn} can be determined by solving the coefficients D_{mn}^i in Eq. (5.20) from the set of linear equations (4.8)–(4.12) as described at the end of the previous section. In the next sections these numbers will be determined in order to examine the effective viscosity for simple $N=1$ arrays.

VI. CUBIC LATTICES

It is the purpose of the present section to compare our results for the effective viscosity for cubic lattices to known results for these systems found in the literature. By exploiting the symmetries of cubic lattices Nunan and Keller [36] have shown that the effective viscosity tensor $\boldsymbol{\eta}_e$ for these arrays is of the following form:

$$(\boldsymbol{\eta}_e)_{ijkl} = \frac{1}{2} \eta (1 + \beta) (\delta_{ik} \delta_{jl} + \delta_{il} \delta_{jk} - \frac{2}{3} \delta_{ij} \delta_{kl}) + \eta (\alpha - \beta) (\delta_{ijkl} - \frac{1}{3} \delta_{ij} \delta_{kl}). \quad (6.1)$$

Here the indices i, j, k , and l denote the components with respect to the Cartesian coordinate axes x, y, z , which coincide with the principal axes of the cubic lattice [50]. Moreover, δ_{ijkl} is unity if all indices are equal and zero otherwise. Thus the effective viscosity tensor $\boldsymbol{\eta}_e$ for cubic lattices is determined by only two parameters α and β , which depend on the type of cubic lattice, i.e., sc, bcc, or fcc, and on the volume fraction ϕ . These separate parameters are directly related to the (scalar) viscosities corresponding to imposed linear flows that are oriented in a special way with respect to the cubic axes, as is discussed below. The physical meaning of the parameter β can be interpreted by considering the Couette flow (simple shear flow) specified by the velocity field

$$\mathbf{v}_a(\mathbf{r}) = \dot{\gamma} y \mathbf{e}_x, \quad (6.2)$$

where $\dot{\gamma}$ is called the strain rate coefficient. By definition the rate of strain tensor for this Couette flow satisfies

$$\mathbf{g}_a = \frac{1}{2} \dot{\gamma} (\mathbf{e}_x \mathbf{e}_y + \mathbf{e}_y \mathbf{e}_x) \quad (6.3)$$

and by combining this expression with Eqs. (5.11) and (6.1) it follows that the deviatoric stress is given by

$$\boldsymbol{\sigma}_d = 2 \eta (1 + \beta) \mathbf{g}_a. \quad (6.4)$$

Thus the stress has only two nonzero components, $(\boldsymbol{\sigma}_d)_{xy}$ and $(\boldsymbol{\sigma}_d)_{yx} = (\boldsymbol{\sigma}_d)_{xy}$, that can be accessed experimentally by measuring the tangential force on a bounding wall (in a Couette apparatus) which is parallel to the shear flow. According to convention the relative shear viscosity η_r that corresponds to the shear flow in Eq. (6.2) is defined by

$$\eta_r = \frac{(\boldsymbol{\sigma}_d)_{xy}}{\eta \dot{\gamma}}, \quad (6.5)$$

and it is found from Eqs. (6.3) and (6.4) that the relative viscosity is related to the parameter β by the simple formula

$$\eta_r = 1 + \beta. \quad (6.6)$$

The parameter α corresponds to *normal stresses* that are generated, for instance, in a uniaxial straining flow given by $\mathbf{v}_a(\mathbf{r}) = \dot{\epsilon} \mathbf{g}_a \cdot \mathbf{r}$ with the rate of strain tensor

$$\mathbf{g}_a = \dot{\epsilon} (\mathbf{e}_z \mathbf{e}_z - \frac{1}{2} \mathbf{e}_x \mathbf{e}_x - \frac{1}{2} \mathbf{e}_y \mathbf{e}_y). \quad (6.7)$$

Here $\dot{\epsilon}$ is called the *extensional velocity*. It can be seen that the velocity field $\mathbf{v}_a(\mathbf{r})$ corresponds to an irrotational shear flow that is axisymmetric (uniaxial) with respect to the z axis. Also, for this special flow it follows, analogously to Eq. (6.4), that the relation between the deviatoric stress and the rate of strain is given by a scalar, as

$$\boldsymbol{\sigma}_d = 2 \eta (1 + \alpha) \mathbf{g}_a. \quad (6.8)$$

It is seen that this stress tensor has only normal (diagonal) components $(\boldsymbol{\sigma}_d)_{xx}$, $(\boldsymbol{\sigma}_d)_{yy} = (\boldsymbol{\sigma}_d)_{xx}$, and $(\boldsymbol{\sigma}_d)_{zz}$. With re-

gard to experiments it is relevant to consider the first and the second normal stress differences, $[(\boldsymbol{\sigma}_d)_{zz} - (\boldsymbol{\sigma}_d)_{xx}]$ and $[(\boldsymbol{\sigma}_d)_{xx} - (\boldsymbol{\sigma}_d)_{yy}]$, respectively. Clearly, the second normal stress difference is vanishing by virtue of symmetry, while the first is proportional to the extensional velocity $\dot{\epsilon}$, according to Eqs. (6.7) and (6.8). The (dimensionless) coefficient in this relation is called the *extensional viscosity* η_{ext} , and is defined by

$$\eta_{\text{ext}} = \frac{(\boldsymbol{\sigma}_d)_{zz} - (\boldsymbol{\sigma}_d)_{xx}}{\eta \dot{\epsilon}}. \quad (6.9)$$

It follows by combination of the above identity with Eqs. (5.11), (6.1), (6.7), and (6.8) that the extensional viscosity is directly related to the viscosity parameter α as

$$\eta_{\text{ext}} = 3(1 + \alpha). \quad (6.10)$$

More generally, it can be inferred by inspection of the effective viscosity tensor that the viscosity parameter (corresponding to a certain stress component, or stress difference, analogous to η_r and η_{ext}) is proportional to $(1 + \alpha)$ for a shear flow whose principal axes [51] are parallel to the axes of the cubic lattice, while it is proportional to $(1 + \beta)$ when the principal axes are at 45° to the cube axes. For any other type of shear the corresponding viscosity parameter is a linear combination of α and β , which follows by application of the viscosity tensor $\boldsymbol{\eta}_e$.

In order to determine α and β it is noted that

$$\alpha = M_{0,0} = M_{2,2}, \quad (6.11a)$$

$$\beta = M_{-2,-2} = M_{-1,-1} = M_{1,1}, \quad (6.11b)$$

where the matrix elements M_{mn} for $m, n \in \{-2, -1, 0, 1, 2\}$ are defined by Eq. (5.15). The above relations can be straightforwardly derived by substitution of Eq. (6.1) for $\boldsymbol{\eta}_e$ into Eq. (5.21). It is furthermore found that all off-diagonal elements M_{mn} are vanishing. The nonzero elements in Eq. (6.11), and thereby α and β , can be determined for the three cubic lattice types by solving the set of linear equations as expounded at the end of the previous section. Restricting ourselves to the equations for truncation level $L=2$ and performing elementary algebraic manipulations we get asymptotic expansions of the form

$$\alpha = \frac{5}{2} \phi [1 + A_\alpha \phi + B_\alpha \phi^{5/3} + O(\phi^{10/3})]^{-1}, \quad (6.12a)$$

$$\beta = \frac{5}{2} \phi [1 + A_\beta \phi + B_\beta \phi^{5/3} + O(\phi^{10/3})]^{-1}. \quad (6.12b)$$

Here the coefficients A_α , B_α , A_β , and B_β can be expressed in terms of lattice sums that can be computed numerically following the method expounded in article I. Expansions similar to those in Eq. (6.12) were previously derived by Zuzovsky *et al.* [48,52], by a generalization of the periodic Green's function method of Hasimoto [53]. In their expressions the unknown higher-order terms are of $O(\phi^{7/3})$, instead of the $O(\phi^{10/3})$ given in Eq. (6.12). It is noted, however, that this discrepancy can be removed by increasing the truncation level. The coefficients A_α , B_α , A_β , and B_β are compared in Table I to the corresponding coefficients in the expansions of Zuzovsky *et al.* and also with those found by

TABLE I. Coefficients in the asymptotic expansions (6.12) appropriate for the viscosity parameters α and β for dilute cubic arrays of spheres, compared to the previous results of Zuzovsky [52] and of Kapral and Bedeaux [34].

		Present calculations	Zuzovsky	Kapral and Bedeaux
sc	A_α	-3.78699	-3.793	-3.787
	B_α	3.42673	3.428	
	A_β	0.85800	0.8620	0.858
	B_β	-2.28448	-2.286	
bcc	A_α	-0.14079	-0.141	-0.141
	B_α	-1.07874	-1.08	
	A_β	-1.57281	-1.573	-1.573
fcc	B_β	0.71916	0.718	
	A_α	-0.23611	-0.237	-0.236
	B_α	-0.82315	-0.822	
	A_β	-1.50926	-1.508	-1.509
	B_β	0.54877	0.548	

Kapral and Bedeaux [34]. The latter authors have calculated the coefficients A_α and A_β as an application of the scheme developed by Bedeaux *et al.* [54], and their results agree with ours to all decimal places quoted. There is a small discrepancy with some of the coefficients provided by Zuzovsky. The origin of these differences is not clear, but they are numerically insignificant, on the order of a few parts in one thousand. Nevertheless, the validity of the claim by Zuzovsky *et al.* that their coefficients are exact while those reported by Kapral and Bedeaux are only approximate may be disputed on the basis of the comparison with our converged computations. The suitability of the asymptotic expansions (6.12) is obviously restricted to dilute arrays. Nunan and Keller [36] reported numerical results for α and β appropriate for the complete range of volume fractions. Their computations are based on a Galerkin technique previously introduced by Zick and Homay [55] in a study of the drag coefficient for cubic arrays (a detailed discussion of drag coefficients can be found in Ref. [56]). On basis of their data for the three cubic lattice types Nunan and Keller conclude that the low- ϕ expansions found by Zuzovsky *et al.* are accurate to within 0.2% for concentrations up to approximately 25% that of close packing, and to within 5% for concentrations up to approximately 50% that of close packing. These accuracies also hold for our expansions, which show only insignificant differences from those of Zuzovsky *et al.*, as can be checked by substitution of the coefficients given in Table I into the expansions (6.12). The viscosity parameters for sc arrays were also calculated by Ladd [57] on the basis of a numerical implementation of the theory of Mazur and van Saarloos to describe many-body hydrodynamic interactions in suspensions [58]. In order to examine the correctness and accuracy of our method to determine the viscosities of spatially periodic arrays in general, we have calculated α and β for cubic lattices at various concentrations ϕ . In Table II the results, indicated by the letter H for each concentration, are compared to those of Ladd (L) and of Nunan and Keller (N). Data that have been measured from Fig. 2 in Ref. [36] are indicated by boldface. All these results are found to

TABLE II. Viscosity parameters α and β as functions of volume fraction ϕ for a sc lattice. Converged numerical results obtained by our method (H) are compared to the numerical data of Ladd [57] (L) and of Nunan and Keller [36] (N). Bold data are measured from Fig. 2 in Ref. [36].

ϕ	Methods	α	β
0.01	H	0.025 941	0.024 813
	L	0.025 942	0.024 814
	N	0.025 941	0.024 813
0.12	H	0.465 796	0.290 025
	L	0.465 80	0.290 03
	N	0.465 80	0.289 95
0.24	H	1.522 857	0.613 821
	L	1.522 8	0.613 81
	N	1.522 8	0.613 06
0.32	H	3.025 744	0.896 926
	L	3.025 7	0.896 9
	N	3.026	
0.40	H	6.457 823	1.312 428
	L	6.453	1.312 3
	N	6.454 1	1.32±0.02
0.44	H	10.487 711	1.634 516
	L	10.43	1.634 3
0.46	H	14.292 654	1.858 631
	N	14.0	1.86±0.02
0.49	H	28.038 95	2.378 24
	N	24	

compare excellently, with differences of at most a few parts in ten thousand if concentrations are below $\phi=0.46$ (except for the β value at $\phi=0.40$ that has been determined graphically). As the concentration approaches that of close packing ($\phi_{cp} \approx 0.524$) the accuracy of the data of Nunan and Keller and of Ladd is seen to decrease rapidly. This is mainly caused by the inadequacy of a necessarily finite number of basis functions (as in our method) to describe the flow through the array of spheres. For high concentrations Nunan and Keller indicate that their computed estimates are sometimes too low. Moreover it can be seen in Table 1 of their paper [36] that the numerical result for α at $\phi=0.49$ shows oscillation as the number of basis polynomials (analogous to our L) is increased. It is likely, therefore, that the value of 24 as quoted in Table II is not converged and should actually be higher, which also explains the relatively large difference with our (fully converged) result. An additional error in the calculations of Nunan and Keller is introduced by the truncation in the lattice sums (these sums are different from ours) which can be significant at large concentrations, as mentioned in their article. It seems that they did not use an efficient technique to calculate the lattice sums, such as the Ewald-like summation expounded in article I, because these computations consumed the preponderance of CPU time needed to determine the viscosity parameters. In our case the lattice sums (which are calculated only once for each of the three cubic lattices) take an insignificant amount of CPU time in comparison to the time needed to solve the set of linear equations. Moreover, it is important to appreciate that accurate computations for higher concentrations require

higher-order lattice sums, and in our case it has been verified that these sums converged to the correct values by comparing the results of our Ewald-like technique with the results that follow by direct summation of the lattice sums (these sums are defined in article I). Having established the main reasons for the major discrepancies between our results and those of Nunan and Keller, and given the excellent correspondence with their data as well as with those of Ladd for concentrations up to approximately 85% that of close packing, it can be concluded that the present method to determine the effective viscosities indeed works correctly and yields accurate results.

To examine the performance of our numerical scheme for computations of viscosities at very high concentrations it is found worthwhile to compare our data to the asymptotic expansions for cubic lattices as derived by Nunan and Keller on the basis of lubrication theory. These formulas, in terms of the small parameter ϵ defined by $\epsilon = 1 - (\phi/\phi_{cp})^{1/3}$, are as follows.

For sc lattices,

$$\alpha = \frac{3}{16}\pi\epsilon^{-1} + \frac{27}{80}\pi\ln\epsilon^{-1} + \tilde{C}_\alpha + \tilde{D}_\alpha\epsilon\ln\epsilon^{-1} + O(\epsilon), \quad (6.13a)$$

$$\beta = \frac{1}{4}\pi\ln\epsilon^{-1} + \tilde{C}_\beta + \tilde{D}_\beta\epsilon\ln\epsilon^{-1} + O(\epsilon). \quad (6.13b)$$

For bcc lattices,

$$\alpha = \frac{1}{4}\sqrt{3}\pi\ln\epsilon^{-1} + \tilde{C}_\alpha + \tilde{D}_\alpha\epsilon\ln\epsilon^{-1} + O(\epsilon), \quad (6.14a)$$

$$\beta = \frac{1}{8}\sqrt{3}\pi\epsilon^{-1} + \frac{37}{120}\sqrt{3}\pi\ln\epsilon^{-1} + \tilde{C}_\beta + \tilde{D}_\beta\epsilon\ln\epsilon^{-1} + O(\epsilon). \quad (6.14b)$$

For fcc lattices,

$$\alpha = \frac{3}{32}\sqrt{2}\pi\epsilon^{-1} + \frac{87}{160}\sqrt{2}\pi\ln\epsilon^{-1} + \tilde{C}_\alpha + \tilde{D}_\alpha\epsilon\ln\epsilon^{-1} + O(\epsilon), \quad (6.15a)$$

$$\beta = \frac{3}{16}\sqrt{2}\pi\epsilon^{-1} + \frac{47}{80}\sqrt{2}\pi\ln\epsilon^{-1} + \tilde{C}_\beta + \tilde{D}_\beta\epsilon\ln\epsilon^{-1} + O(\epsilon). \quad (6.15b)$$

In the above equations the coefficients \tilde{C}_α , \tilde{D}_α , \tilde{C}_β , and \tilde{D}_β are different for sc, bcc, and fcc lattices. In order to determine, for example, \tilde{C}_α and \tilde{D}_α for sc lattices Nunan and Keller wrote

$$\alpha - \left(\frac{3}{16}\pi\epsilon^{-1} + \frac{27}{80}\pi\ln\epsilon^{-1}\right) = \tilde{C}_\alpha + \tilde{D}_\alpha\epsilon\ln\epsilon^{-1} + O(\epsilon), \quad (6.16)$$

and by plotting the computed value of the left side of this equation against $\epsilon\ln\epsilon^{-1}$ the coefficients of interest could be found from the intercept and slope of a line drawn through the plotted data for small ϵ (high concentrations).

In the following discussion $\tilde{\alpha}$ will be written as a shorthand notation for the singular terms of α appropriate for the particular cubic lattice type under consideration. The notation $\tilde{\beta}$ is defined in an analogous way. Thus for the sc array $\tilde{\alpha}$ indicates the singular terms between parentheses in Eq. (6.16).

Following the above procedure we have fitted the unknown coefficients to our numerical data. For the sc array

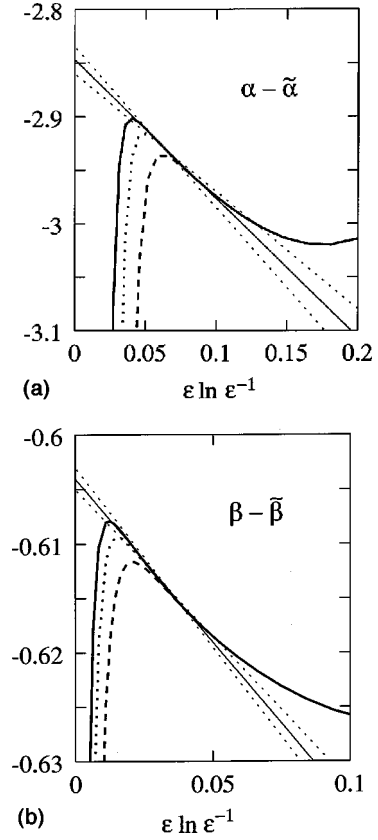


FIG. 1. Differences $(\alpha - \tilde{\alpha})$ (a) and $(\beta - \tilde{\beta})$ (b) versus $\epsilon\ln\epsilon^{-1}$ for a sc lattice. Computations are shown for $L=40$ (dashed curve), $L=50$ (dotted curve), and $L=60$ (solid curve). Dotted straight lines give an indication of the deviations around the best fit (solid straight line).

Fig. 1 shows the residuals $(\alpha - \tilde{\alpha})$ (a) and $(\beta - \tilde{\beta})$ (b) versus $\epsilon\ln\epsilon^{-1}$. Curves represent the results calculated for $L=40$ (dashed curve), $L=50$ (dotted curve), and $L=60$ (solid curve). For the smallest values of ϵ the results have clearly not converged, whereas for the larger ϵ the terms of $O(\epsilon)$ are becoming prominent [see Eq. (6.16)], but in an intermediate range it is possible to resolve a distinct linear behavior of the curves. In this intermediate range the straight solid line is fitted to the curve, within an error that is indicated by the two dotted lines. In an analogous way the residuals $(\alpha - \tilde{\alpha})$ and $(\beta - \tilde{\beta})$ for the bcc lattice are shown in Fig. 2, and for the fcc lattice in Fig. 3. In Table III the coefficients corresponding to our fitting lines, denoted as C_α , D_α , C_β , D_β , are compared to the fitting constants of Nunan and Keller, \tilde{C}_α , \tilde{D}_α , \tilde{C}_β , \tilde{D}_β , respectively. It is immediately seen in this table that the sign of Nunan and Keller's coefficients is systematically opposite to the sign of our coefficients. Because we are certain that the sign of our coefficients is correct the conclusion follows that Nunan and Keller must have mistakenly fitted the line for $(\tilde{\alpha} - \alpha)$ instead of $(\alpha - \tilde{\alpha})$. The sign of the other coefficients reported by Nunan and Keller is incorrect for the same reason. For the bcc or fcc lattice Nunan and Keller find that their graphs of $(\alpha - \tilde{\alpha})$ exhibit definite linear behavior as ϵ becomes small, so that the coefficients \tilde{C}_α and \tilde{D}_α can be determined with confidence. But in the other cases their estimates of the coefficients are not as

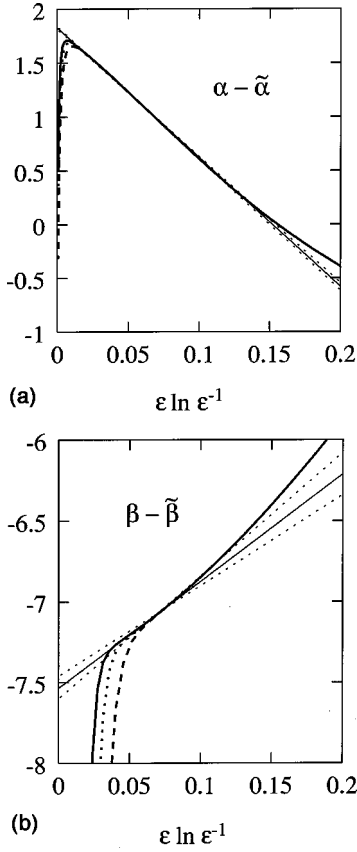


FIG. 2. Differences $(\alpha - \tilde{\alpha})$ (a) and $(\beta - \tilde{\beta})$ (b) versus $\epsilon \ln \epsilon^{-1}$ for a bcc lattice. The various lines and curves are as for the sc case shown in Fig. 1.

reliable, and in the case of β for a fcc lattice no estimate could be made. It is found by inspection of Table III that our results are strikingly different (apart from the trivial minus sign) precisely in the cases where they question the accuracy of their data, with the exception of the coefficients \tilde{C}_α and \tilde{C}_β for a sc lattice, which show reasonable agreement with our corresponding coefficients C_α and C_β . It is noted that these coefficients are somewhat larger in magnitude than our C_α and C_β for the sc lattice (again disregarding signs) as can be expected, because for these high concentrations ($\phi \approx 0.48$ for $\epsilon \ln \epsilon^{-1} = 0.1$) Nunan and Keller's numerical results have not fully converged and, as mentioned before, there was strong evidence of a downward bias in these computations for all cubic lattices. Although Nunan and Keller have not presented curves for $(\alpha - \tilde{\alpha})$ and $(\beta - \tilde{\beta})$ it seems, on the basis of our findings, that they overestimated the accuracy of their numerical results and therefore also of their fitting parameters.

Having determined the constant and $\epsilon \ln \epsilon^{-1}$ terms in the expansions (6.13)–(6.15) with a reasonable accuracy, it is interesting to observe that terms of $O(1)$ (that is, constant and higher-order terms) are not negligible as compared to the singular terms, even for the rather high concentrations corresponding to Figs. 1–3 (for all cubic lattices $0.78 \leq \phi/\phi_{cp} \leq 0.97$ for $0.05 < \epsilon \ln \epsilon^{-1} < 0.2$). This can be seen in Fig. 4, where $(\alpha - \tilde{\alpha})/\tilde{\alpha}$ (thick curves) and $(\beta - \tilde{\beta})/\tilde{\beta}$ (thin curves) are plotted as functions of $\epsilon \ln \epsilon^{-1}$, for sc (a), bcc (b), and fcc (c) lattices. As in Figs. 1–3 the data are given for truncation

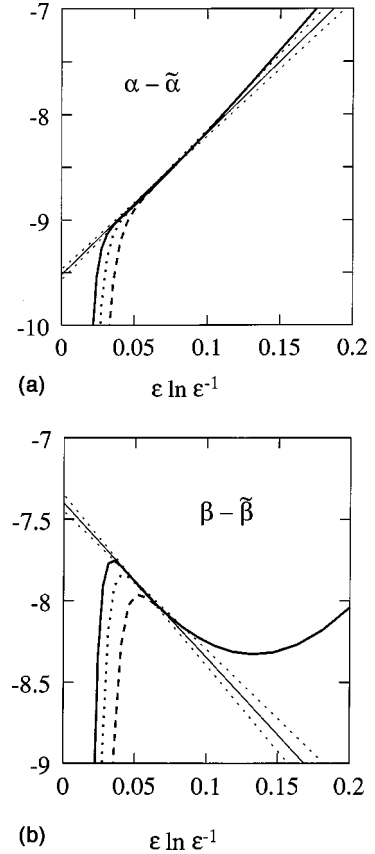


FIG. 3. Differences $(\alpha - \tilde{\alpha})$ (a) and $(\beta - \tilde{\beta})$ (b) versus $\epsilon \ln \epsilon^{-1}$ for a fcc lattice. The different lines and curves are explained in Fig. 1.

levels $L=40$ (dashed curves), $L=50$ (dotted), and $L=60$ (solid). Note that curves for different truncation levels cannot be distinguished in (a) and for $(\alpha - \tilde{\alpha})/\tilde{\alpha}$ as given in (b). For all cubic lattice types the relative magnitude of the $O(1)$ terms varies from 10% to 30% for $0.05 < \epsilon \ln \epsilon^{-1} < 0.2$ and, as follows from Figs. 1–3, the predominant part of these higher-order terms is represented by the constant terms and the terms proportional to $\epsilon \ln \epsilon^{-1}$ that have been determined by fitting. Obviously, when concentrations are decreasing the terms of $O(\epsilon)$ will become important, but the lubrication-theory expansions up to the $\epsilon \ln \epsilon^{-1}$ terms (including our

TABLE III. Fitting coefficients C_α , D_α , C_β , and D_β appropriate for the lubrication formulas (6.13)–(6.15) for sc, bcc, and fcc lattices. Previous results by Nunan and Keller [36] are denoted as \tilde{C}_α , \tilde{D}_α , \tilde{C}_β , and \tilde{D}_β .

	sc	bcc	fcc
C_α	-2.85 ± 0.02	1.83 ± 0.02	-9.54 ± 0.05
\tilde{C}_α	3.1	-1.73	9.7
D_α	-1.3 ± 0.2	-12.0 ± 0.3	14 ± 1
\tilde{D}_α	0.25	12.3	-15.5
C_β	-0.604 ± 0.001	-7.5 ± 0.1	-7.40 ± 0.05
\tilde{C}_β	0.63	12.8	
D_β	-0.30 ± 0.03	6 ± 1	-9 ± 1
\tilde{D}_β	0.0	-35	

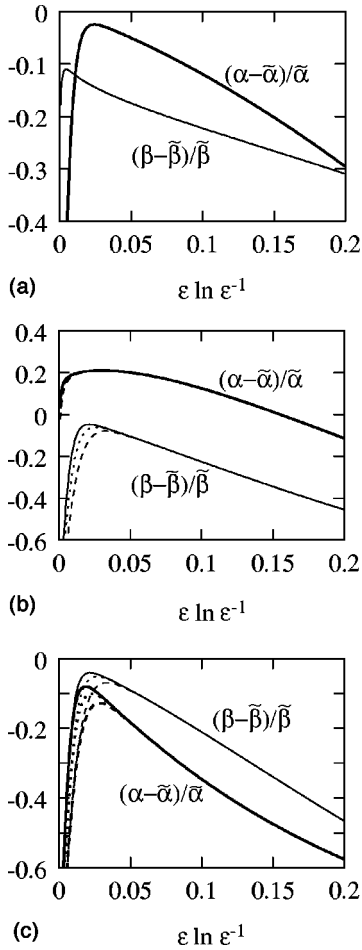


FIG. 4. Relative differences $(\alpha - \tilde{\alpha})/\tilde{\alpha}$ (thick curves) and $(\beta - \tilde{\beta})/\tilde{\beta}$ (thin curves) versus $\epsilon \ln \epsilon^{-1}$ for sc (a), bcc (b), and fcc (c) lattices. Truncation levels are $L=40$ (dashed curves), $L=50$ (dotted), and $L=60$ (solid). Note that curves for different truncation levels are indistinguishable in (a) and for $(\alpha - \tilde{\alpha})/\tilde{\alpha}$ in (b).

fitting coefficients) are reasonably accurate even at moderate volume fractions, as is shown for the sc case in Fig. 5. Our converged numerical results for α (a) and β (c), as a function of the volume fraction ϕ , are given by the solid curves. The thick dotted curves indicated by 0 represent the singular terms $\tilde{\alpha}$ and $\tilde{\beta}$, respectively, while those indicated by + and \square show the expansions (6.13) up to and including the $\epsilon \ln \epsilon^{-1}$ terms with coefficients as provided by Nunan and Keller (+) and with coefficients taken with opposite sign (\square). As has been mentioned before, the signs of all fitting coefficients of Nunan and Keller should be changed, which indeed yields a definite improvement to the plain lubrication results (0). Their modified fitting results (\square) seem to be somewhat better than the curves that correspond to our fitting coefficients (dashed curves) but this is only for low to intermediate concentrations, and in that range the low- ϕ expansions (6.12) (dotted curves) provide a much greater accuracy, as can be seen in Fig. 5(a) (for α) and Fig. 5(c) (for β). These low- ϕ expansions have been plotted here using the coefficients $A_\alpha, B_\alpha, A_\beta, B_\beta$ as determined in this work (see Table I) but the curves would not be visibly different for the coefficients reported by Zuzovsky [52]. Numerical data of Nunan and Keller are shown as diamonds (\diamond). Their results

for α are as given in Table II whereas the results for β have been measured from Fig. 2 in Ref. [36] [with measuring errors smaller than the size of the \diamond symbols in Figs. 5(c) and 5(d)]. These data are all on our curves, except for α at $\phi=0.49$ which is somewhat below our result, as can be seen in Fig. 5(b). The circles show some results obtained by the Stokesian dynamics approach (Brady *et al.* [59]) which is devised so as to be accurate in the limits of very small and extremely high concentrations. At intermediate concentrations the Stokesian dynamics computations overpredict the viscosity parameters, as was already mentioned in Ref. [59]. Note that the viscosity parameters diverge as close packing is approached, as is clearly seen in Fig. 5(b) and Fig. 5(d). The close packing concentration is $\phi_{cp} \approx 0.524$, as indicated by the vertical dotted line.

In a similar way results for a bcc lattice are plotted in Fig. 6, where the dashed curves show the lubrication formulas (6.14) corresponding to our fitting coefficients. The fitting error for β is indicated by the deviations between the three dashed curves in (b). As for the sc case these modified lubrication formulas yield a considerable improvement on the pure singular part of Eqs. (6.14) (0), and for α (a) our lowest fitting results are close to those of Nunan and Keller, which are shown by the thick dotted curves indicated by the symbol \square . Note that the sign of their coefficients has been altered. For the viscosity parameter β , as shown in Fig. 6(b), there is a marked discrepancy between our numerical results and those of Nunan and Keller at higher concentrations. This is caused by the fact that their data have not converged, which also explains the negative bias of their fitting results (\square) as compared to our converged numerical data given by the solid curve in (b). Even larger discrepancies between our numerical computations and those of Nunan and Keller are found for β corresponding to fcc lattices, as shown in Fig. 7(b). In that case they were not able to determine the fitting coefficients with a reasonable accuracy. It is also noticed that our fitting result, as given by the dashed curve in Fig. 7(b), yields only a very poor approximation in a wide range of intermediate to high volume fractions.

Observing the results shown in this section, it can be concluded that the present method is effective in calculating viscosity parameters for cubic arrays, and good accuracy can be retained even for relatively high concentrations. This effectiveness is not limited to cubic arrays, as the lattice sums appropriate for various other types of array can be straightforwardly (and rapidly) computed. The use of rapidly converging expressions for these lattice sums (like those presented in article I) is advocated, as it seems that neglect thereof has unnecessarily affected the calculations of Nunan and Keller in an adverse way. In the next section the effective viscosity is examined for simple tetragonal (st) lattices and the results are interpreted in relation to various possible structures of the st type.

VII. SIMPLE TETRAGONAL LATTICES

Simple tetragonal lattices may be characterized as sc lattices that are compressed or elongated along one of their axes. As in the previous section the three orthogonal axes are chosen so as to coincide with the coordinate system xyz , with z the direction of elongation. The st lattice parameters

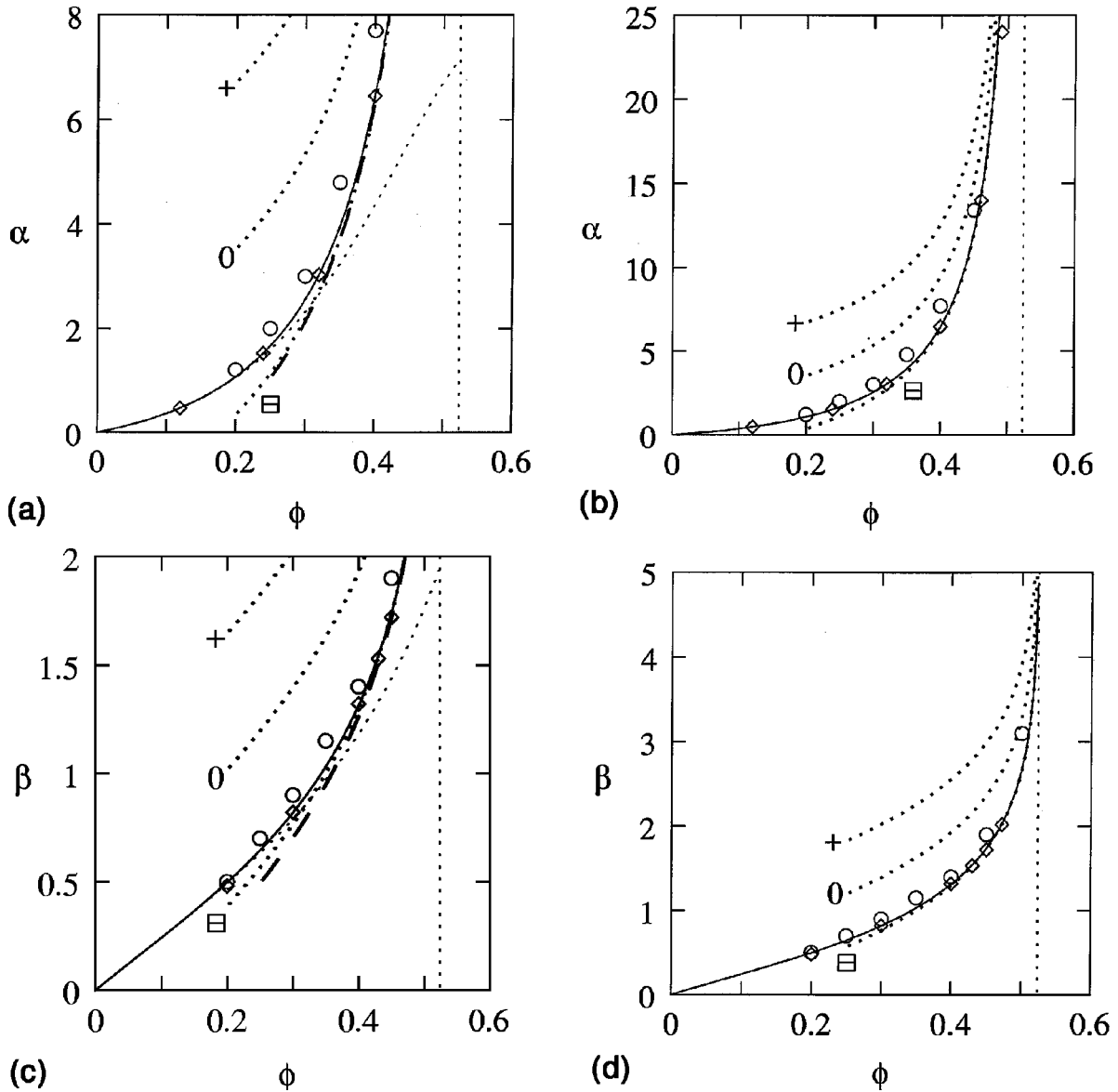


FIG. 5. Viscosity parameters α and β for sc arrays, plotted against the volume fraction ϕ . Various results shown in (a)–(d) are indicated as follows. Solid curves, our converged numerical data; circles, Stokesian dynamics [59]; diamonds (\diamond), numerical data from Nunan and Keller [36]. The thick dotted curves indicated by 0 represent $\tilde{\alpha}$ [(a),(b)] and $\tilde{\beta}$ [(c),(d)] while those marked with + and \boxminus show the expansions (6.13) up to and including the $\epsilon \ln \epsilon^{-1}$ terms with coefficients given in Ref. [36] (+) and with coefficients taken with opposite sign (\boxminus). Low- ϕ expansions (6.12) are indicated by the thin dotted lines for α (a) and β (c) including our coefficients given in Table I; dashed curves in (a) and (c) represent the lubrication formulas (6.13) including our fitting coefficients in Table III. Notice the different scales in (a)–(d).

along these respective axes are given by h_x , $h_y = h_x$, and h_z . Obviously this type of array possesses less symmetry than cubic arrays, and it is not possible, therefore, to reduce the computational effort to the same degree (see article I for details). However, by changing the aspect ratio $f = h_z/h_x$ of a st lattice, a wide range of different structures can be considered. For these simple structures the effective viscosity can be interpreted in a straightforward way, as is shown below, and this can be useful in understanding the rheological behavior of ordered hard-sphere suspensions (see, e.g., Refs. [21,60,61,22,62,63]). In the next section some of our numerical results are compared to recent experimental data.

The present section focuses on the interpretation of the effective viscosity as calculated for st lattices submitted to

Couette flow (simple shear flow) as depicted in Fig. 8(a) where the arrows indicate the ambient velocity field (6.2) which is parallel to the x axis [the Cartesian axes are plotted in (b)]. Under the influence of this shear flow the spheres rotate as indicated by the curved arrows in (b) and (c). The effective shear viscosity corresponding to this orientation of the flow is given by η_r in Eq. (6.5). Analogously to the sc case it is found convenient to write $\eta_r = 1 + \beta_z$ where the parameter $\beta_z = M_{-2,-2}$ can be determined from the set of linear equations suitable for the st lattice under consideration. The viscosity parameter β_z is shown in Fig. 9 against the aspect ratio $f = h_z/h_x$ for a volume fraction of $\phi = 0.3$. This moderate concentration is sufficient to explain the characteristic structural dependence of the viscosity in a qualita-

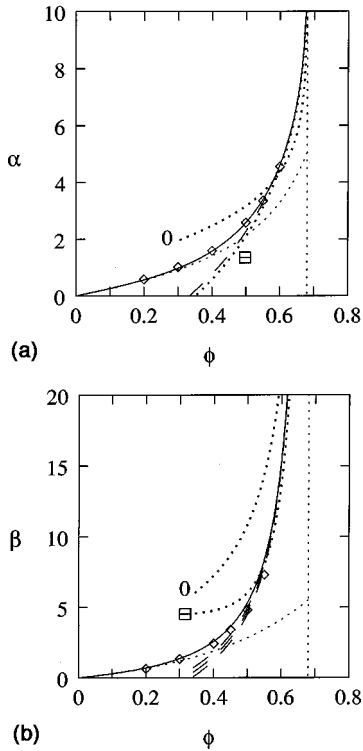


FIG. 6. Viscosity parameters α (a) and β (b) versus the volume fraction ϕ for bcc lattices. The three dashed curves in (b) show the lubrication formula for β in (6.14) including our fitting coefficients, where the fitting error is indicated by the deviations between these three curves. Other symbols and lines are as in Fig. 5.

tive way. This behavior has been shown to be roughly the same for all possible volume fractions. When the spheres are touching in the z direction, as depicted in Fig. 8(b), the aspect ratio reaches a minimal value $f=f_{\min}$ as indicated by the left vertical dashed line in Fig. 9, and for this situation the viscosity rapidly converges (as a function of L) to a finite value. For a given volume fraction ϕ the minimal aspect ratio is given by

$$f_{\min} = \sqrt{\frac{6\phi}{\pi}} \quad (7.1)$$

and for $\phi=0.3$, as considered here, it follows that $f_{\min} \approx 0.76$. We have also calculated the velocities and angular velocities of the particles *relative to the ambient flow*, as given by \tilde{U}_n and $\tilde{\Omega}_n$ in Eq. (4.5) (where $n=0$ as we are considering $N=1$) and these are found to be vanishing, independent of the aspect ratio f . It is worthwhile to appreciate that the *absolute* motions given by U_n and Ω_n are nonzero. Thus, all spheres move along with the shear flow in exactly the same way as can be derived for a single isolated sphere. Moreover, our numerical computations show that this also applies if the spheres are arranged on a cubic lattice. In fact, for cubic lattices this property was explained by Nunan and Keller [36] and it appears that this property is retained for st lattices which are oriented with respect to the shear flow as considered here [64].

As the aspect ratio is increased the structure becomes simple cubic at $f=1$ where β_z in Fig. 9 indeed reaches the correct value, which has also been computed following a

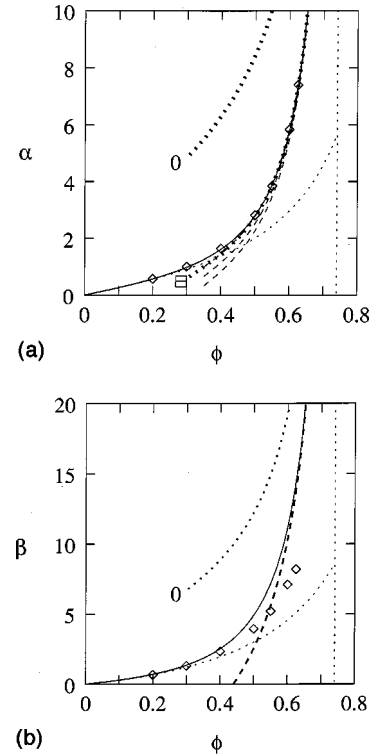


FIG. 7. Viscosity parameters α (a) and β (b) versus the volume fraction ϕ for fcc lattices. The three dashed curves in (a) show the lubrication formula (6.15) corresponding to our fitting coefficients, where the fitting error is indicated by the deviations between these three curves. Other symbols and lines are as in Fig. 5.

numerical scheme that is optimized by exploiting cubic symmetry. By further increasing f the separation between spheres becomes larger in the z direction, whereas distances are decreasing in the xOy plane, as can be seen in Fig. 8. Large stresses are produced in the regions between spheres that are neighbors in the xOy plane, and this explains the monotonically increasing behavior of the viscosity parameter as a function of the aspect ratio, as shown in Fig. 9. Finally, the viscosity diverges at $f=f_{\max}$ (as indicated by the right vertical dashed line in Fig. 9) which corresponds to spheres touching in the xOy plane [see Fig. 8(c)]. Here f_{\max} depends on the concentration ϕ according to

$$f_{\max} = \frac{\pi}{6\phi}, \quad (7.2)$$

which yields $f_{\max} \approx 1.75$ for $\phi=0.3$.

For the same tetragonal structures the shear viscosity parameter has been computed that corresponds to a plane of shear coinciding with yOz , as depicted in Fig. 10. This viscosity parameter will be denoted β_x and is plotted versus aspect ratio f in Fig. 11(a). Relative to the shear flow all spheres exhibit the same angular velocity in the x direction, $\tilde{\Omega}_x$. As is inferred by virtue of symmetry, their translational velocity with respect to the ambient flow is found to be zero, as in all other cases mentioned above. The dimensionless fraction $\tilde{\Omega}_x/\dot{\gamma}$ is plotted in Fig. 11(b) versus the aspect ratio f . Here $\dot{\gamma}$ is the shear rate parameter that represents the strength of the shear flow. For the extreme values of the

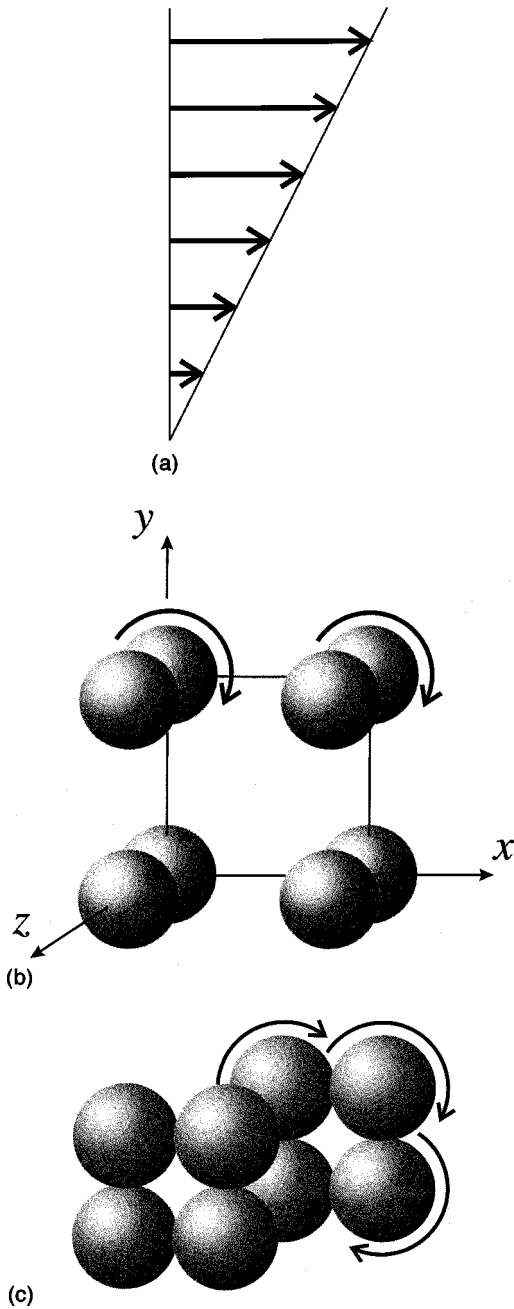


FIG. 8. st arrays of spheres (b) and (c), subject to a Couette flow in the xOy plane, as depicted in (a). The spheres rotate as indicated by the curved arrows in (b) and (c).

aspect ratio $f=f_{\min}$ and $f=f_{\max}$ the spheres are touching, as shown in Figs. 10(b) and 10(c); however, the viscosity parameter β_x is found to converge (slowly) to a finite value. This behavior is closely related to the observation that particles tend to a rolling motion at $f=f_{\min}$ [corresponding to Fig. 10(b)] whereas in the case of $f=f_{\max}$ [Fig. 10(c)] the rotation stops as the spheres form rigid planes that are moving past each other in the y direction. It should be noted that for nonrotating spheres $\bar{\Omega}_x = -\frac{1}{2}\dot{\gamma}$ whereas for rolling spheres $\bar{\Omega}_x = +\frac{1}{2}\dot{\gamma}$. These extreme values ($\pm\frac{1}{2}$) have not been reached in the graph in Fig. 11(b) because the results for touching spheres have not fully converged.

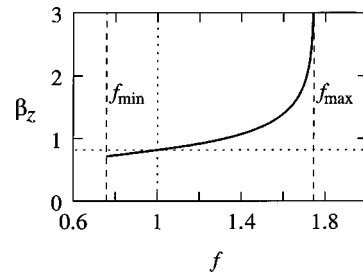


FIG. 9. Viscosity parameter β_z for st lattice at $\phi=0.3$.

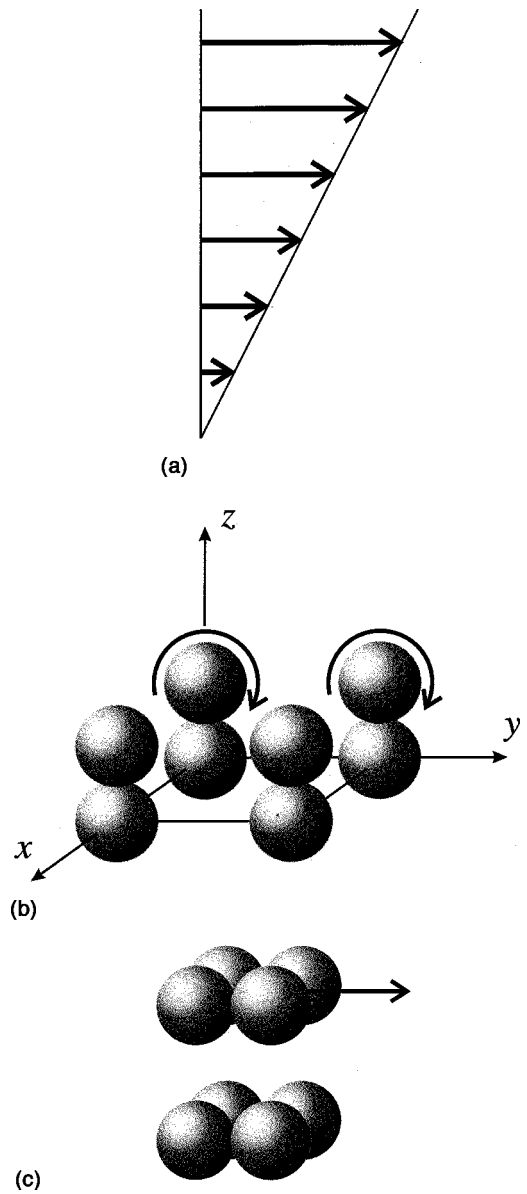


FIG. 10. st arrays of spheres (b) and (c), subject to a Couette flow in the yOz plane, as depicted in (a). In (b) the spheres rotate as indicated by the curved arrows, while in (c) the rotation has stopped and the spheres form close packed planar structures that move past each other in the y direction.

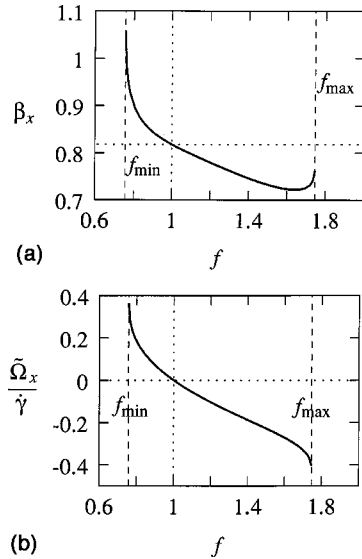


FIG. 11. Viscosity parameter β_x (a) and corresponding relative angular velocity $\tilde{\Omega}_x / \dot{\gamma}$ (b) for st lattice at $\phi=0.3$.

VIII. COMPARISON WITH RHEOLOGICAL EXPERIMENTS

In the past few decades the rheological behavior of colloidal suspensions has been increasingly studied in close relation to the microstructure, and many works report various ordered structures that arise when these systems are subject to different kinds of shear flow (see, e.g., [60,61,63]). As has been indicated in the previous section, a changing microstructure can be responsible for large variations in the effective viscosity.

In recent experiments by Gondret and Petit [21] the viscosity of a hard-sphere suspension is measured by submitting the suspension to an oscillating shear flow. In their experimental setup the suspension consists of glass beads (with diameters in the range $45 \pm 5 \mu\text{m}$ and mass density $\rho_p = 2.5 \text{ g cm}^{-3}$) that are immersed in a viscous fluid ($\eta = 5 \text{ Pa s}$, $\rho = 0.97 \text{ g cm}^{-3}$). This suspension is confined between two parallel solid plates separated by a small gap of size $h = 200 \mu\text{m}$. It should be noted that this gap distance h is only about four times as large as the mean diameter of the beads. The lower plate is fixed and the upper one oscillates in one direction, creating a simple shear flow that satisfies the following specifications: frequency $\nu_s = 200 \text{ Hz}$; amplitude of displacement of the upper plate $x_m \approx 20 \mu\text{m}$; strain rate amplitude $\dot{\gamma}_m = 2\pi\nu_s x_m / h$. Considering the small size of the particles, the high viscosity of the suspending fluid, and the properties of the shear flow, the particle Reynolds number is very small ($\text{Re} \approx 10^{-5}$). Moreover, Brownian forces as well as van der Waals and electrostatic forces between the particles can be neglected, and consequently the particle interactions can be considered as of hydrodynamic origin only. It is observed that, after many oscillations, the initially random suspension reaches an ordered structure. This phenomenon was first reported by Petit and Noetinger and can be ascribed to a secondary flow due to inertial effects induced by the alternating rotation of the particles in the oscillating shear flow [22]. As indicated by the smallness of the Reynolds number these inertial effects are weak, but

not completely vanishing, and this causes the particles to migrate over distances of their own size in a characteristic time of roughly 100 s (as discussed in Ref. [21]); this is effectively the typical time in which the formation of the regular structure has been observed. As was shown in Ref. [21], the viscosity measurements by Gondret and Petit compare reasonably well with the numerical results for sc lattices as reported by Nunan and Keller, for volume fractions up to about 0.5. The main difference between the structures seen in the experiment and the pure sc structure is that the particles in the former are in contact in the direction that is perpendicular to the plane of shear. Although Gondret and Petit were not able to determine the structure with great detail, they assume that it closely resembles a tetragonal lattice. This tetragonal structure, which will be referred to as st1, is depicted in Fig. 12(c) and is oriented with respect to the Couette flow as indicated in (a).

The viscosity parameter β corresponding to this situation was calculated using the method introduced in Sec. V. In Fig. 13 the results (dotted curve) are plotted against the concentration ϕ , on a linear scale (a) and on a logarithmic scale (b). Circles indicate the experimental data corresponding to the disordered suspension as the shear flow has just started. The experimental accuracy is $\pm 10\%$ as shown by the error bars. After a few minutes of shearing the structure is ordered and the viscosity has reached a final value that is considerably lower than in the disordered state (by a factor of ≈ 2). The final viscosity values, shown by the diamond symbols (\diamond) in Fig. 13, are very close to the solid line that represents our calculations for a sc lattice, but the viscosity parameter for the st1 structure (dotted line) shows less correspondence with the experiment. Another candidate for the regular structure observed in the experiment is the st2 array, which is a st structure where particles are touching in the xOy plane, as depicted in Fig. 12(d). When viewed from above, this structure shows a close resemblance to the st1 array depicted in Fig. 12(c). The viscosity parameter β for this st2 structure is shown by the dashed line in Fig. 13, which is below all other results for $\phi \leq 0.25$ but is found to be closer to the experimental data than the results for sc at high concentrations. As compared to the viscosity results for st1 and st2, the results for the sc array best fit the experimental data over the whole range of volume fractions up to sc close packing ($\phi_{\text{cp}} \approx 0.52$). As mentioned above, the sc structure is not what is observed in the experiments, at least not when concentrations are in the range of 0.2 to 0.3 for which clear photographs are available (see Refs. [21,22]). It may be worthwhile to visualize these ordered suspensions at higher concentrations also, and in all three directions, so as to verify the existence of the st2-like structures that are suggested by our findings.

Viscosities have also been measured at concentrations exceeding that for the sc closely packed arrangement. No clear observations are available for these high concentrations, but it is obvious that the corresponding structure cannot be one of those shown in Fig. 12. There are many different arrays of spheres that have concentrations above that for sc close packing, and for some of them we have computed the viscosity parameters corresponding to various directions of the shear. For reasons of brevity only three of the structures considered are depicted in Fig. 14, viz., the bcc (b), bct1 (c), and hexa2 (d) lattices. The hexa2 array consists of (infinite)

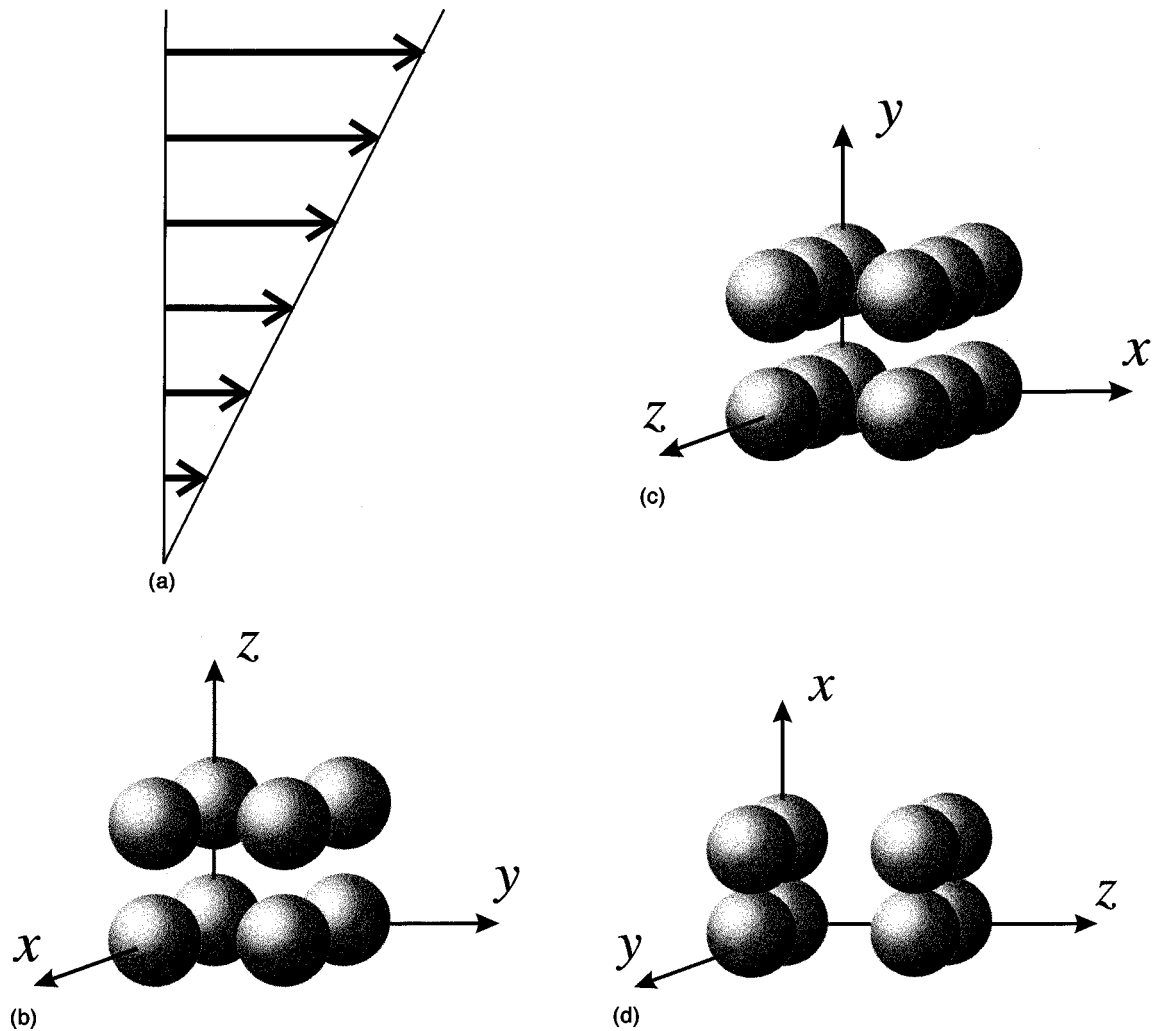


FIG. 12. sc (b), st1 (c), and st2 (d) arrays subject to a Couette flow as depicted in (a).

planes of close packed spheres, which are perpendicular to the direction of the Couette flow shown in (a). For the close packing case [$\phi_{cp} = \pi/(3\sqrt{3}) \approx 0.60$] this hexagonal arrangement was considered by Gondret and Petit [65] as a candidate structure where the spheres are allowed to move in the direction of the flow, whereas for concentrations below close packing the structure is planar, as is also vaguely observed in the experimental case [66].

In Fig. 15 the converged β parameters obtained numerically for the three structures in Fig. 14 are shown on linear (a) and logarithmic (b) scales, as a function of the concentration ϕ . Results for the various structures are represented by the thin dotted curve (hexa2), the thick dotted curve (bct1), and the dashed curve (bcc). Moreover, the calculations for the sc lattice are shown by the solid curve, and vertical lines (the same line types) indicate close packing for all four lattices. The close packing concentration corresponding to bcc is somewhat below that of bct1 (for bcc $\phi_{cp} = \pi\sqrt{3}/8 \approx 0.68$ and for bct $\phi_{cp} = 2\pi/9 \approx 0.70$). The data measured by Gondret and Petit [66] are indicated as in Fig. 13. For increasing concentrations the experimental data show a distinctly different behavior when the volume fraction has passed that of sc close packing, and this is likely due to large changes in the microstructure. The numerical data for the

previously proposed hexa2 structure show a large downward discrepancy with the measurements for the (allegedly) ordered structure for all volume fractions, while the curves for bct1 and bcc lattices also reveal a very different concentration dependence. However, the results for bct1 and bcc are seen to compare reasonably well for some of the higher concentrations, and this correspondence is better than was observed for all other structures that were considered (results for these other structures are not given here), with the exception of the fcc lattice for which results are comparable with those for bct1. It is noted that the viscosity for the fcc array was evaluated here for a Couette flow with yOz as the plane of shear and oriented with respect to the principal axes of the fcc lattice (x, y, z) as depicted in Fig. 16. On the basis of the findings discussed in this section it is proposed that the suspension microstructure in the experiments by Gondret and Petit changes from a st type of arrangement to a bct- or fcc-like arrangement when the volume fraction is raised above that of sc close packing. This proposition may be decided on by experimental verification.

There are several aspects of the experimental situation that have not been taken into account in our calculations, e.g., the fact that only a small number of layers of spheres were contained between the parallel walls in the experimen-

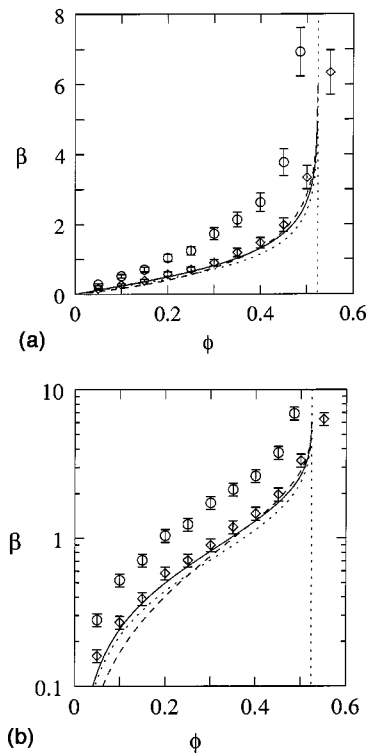


FIG. 13. Viscosity parameter β for various structures plotted on a linear scale (a) and on a logarithmic scale (b) versus the concentration ϕ . Curves show the numerical data for arrays of type sc (solid), st1 (dotted), and st2 (dashed). These structures are oriented relative to the Couette flow as depicted in Fig. 12. The vertical dotted line indicates the close packing concentration for these structures ($\phi_{cp} = \frac{1}{6}\pi$). Experimental data provided by Gondret and Petit [21,66] are shown for disordered (circles) and ordered (\diamond) suspensions where error bars indicate the measuring inaccuracy of $\pm 10\%$.

tal apparatus. Depending on the concentration, this number varies from 3 to 4. Moreover, the structures that are observed after many oscillations of the shear flow still show a definite degree of disorder [21].

IX. CONCLUSION

An exact scheme is presented to determine the 25 independent components of the effective viscosity tensor. In the highly symmetric case of cubic lattices this tensor is characterized by only two viscosity parameters α and β . For these parameters asymptotic expansions have been derived that are appropriate for small volume fractions. These expansions are of the same form as previously found by Zuzovsky *et al.* [48,52] but with slightly different coefficients (differences are below 1%). Although the origin of this discrepancy is unclear we are confident about the correctness of our coefficients, which have fully converged. Moreover, some of the coefficients were previously calculated by Kapral and Bedeaux [34] and these agree with our results (but not with those of Zuzovsky *et al.*) to all decimal places. The viscosity parameters α and β are calculated numerically for the three cubic lattice types and for the whole range of concentrations. For low to intermediate concentrations these results compare excellently with computations of Nunan and Keller [36] and

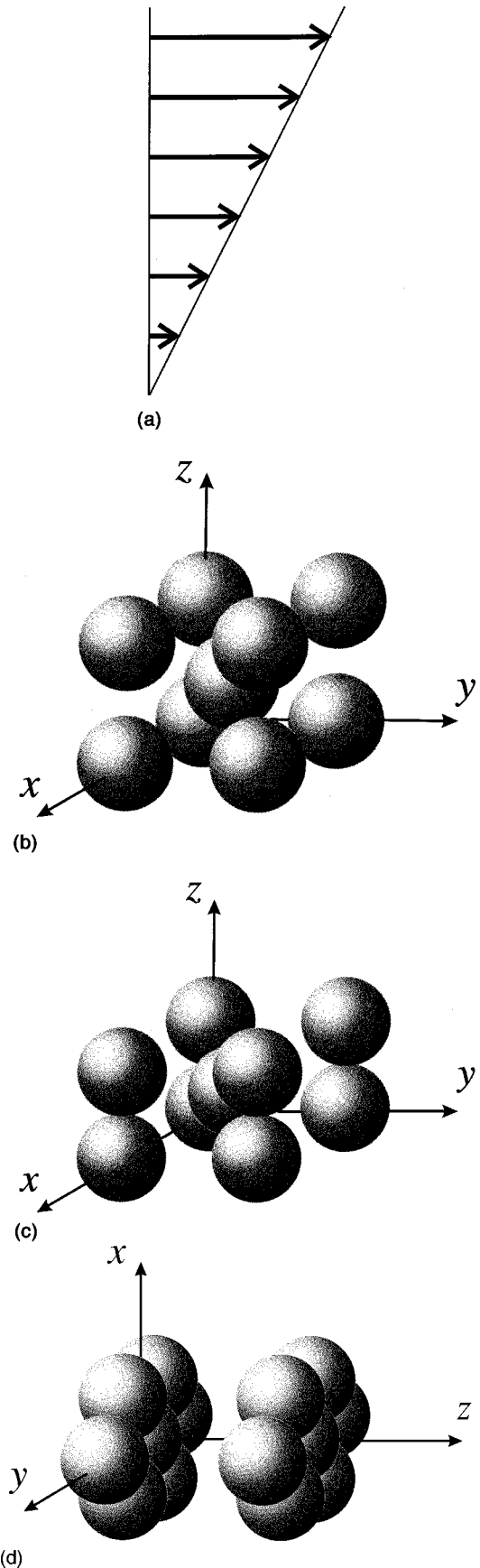


FIG. 14. bcc (b), bct1 (c), and hexa2 (d) arrays submitted to a Couette flow as depicted in (a).

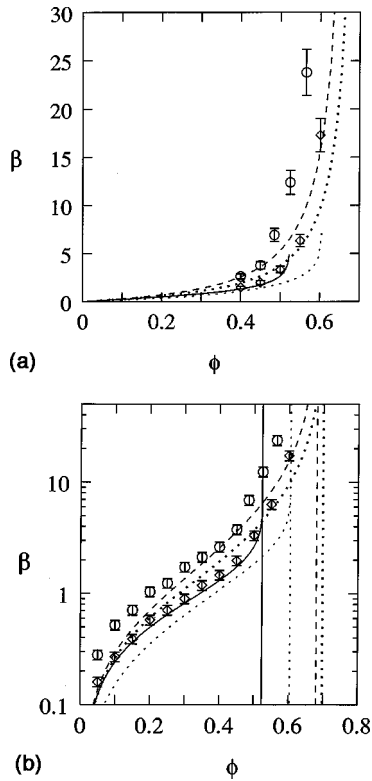


FIG. 15. Shear viscosity β for various structures plotted on linear (a) and logarithmic (b) scales as a function of concentration ϕ . Curves show the numerical data for arrays of type bcc (dashed), bct1 (big dots), sc (solid), and hexa2 (small dots). Vertical lines (same line types) indicate the corresponding close packing concentrations for these structures. Experimental data provided by Gondret and Petit [21,66] are shown for disordered (circles) and ordered (\diamond) suspensions where error bars indicate the measuring inaccuracy of $\pm 10\%$.

also with the data provided by Ladd [57] for the case of a sc lattice. Discrepancies with the data of Nunan and Keller for dense cubic arrays are attributed to the fact that their data have not fully converged.

Asymptotic expansions appropriate for very dense cubic arrays were previously derived by Nunan and Keller on the basis of lubrication theory. Singular terms in these expansions are exactly known, and coefficients of some nonsingular higher-order terms were determined by fitting the expansions to the numerical data for high concentrations. By repeating this fitting procedure on the basis of our converged numerical data we have determined the coefficients of interest. It is shown first that the coefficients reported by Nunan and Keller have the wrong sign, which can be ascribed to a trivial mistake, and second that the accuracy of their coefficients has been overestimated by underestimation of numerical errors. Even at relatively low volume fractions the lubrication theory expansions for α and β (including our numerically obtained coefficients) have proved to be reasonably accurate. Moreover, a combination of these high-density results with the expansions for dilute cubic arrays describes the viscosity parameters rather well over the whole range of volume fractions. Such combined descriptions can be provided by our method for various other lattices (with possibly multiple particles per cell that may have different sizes) and these results may be used to increase the accuracy of fast

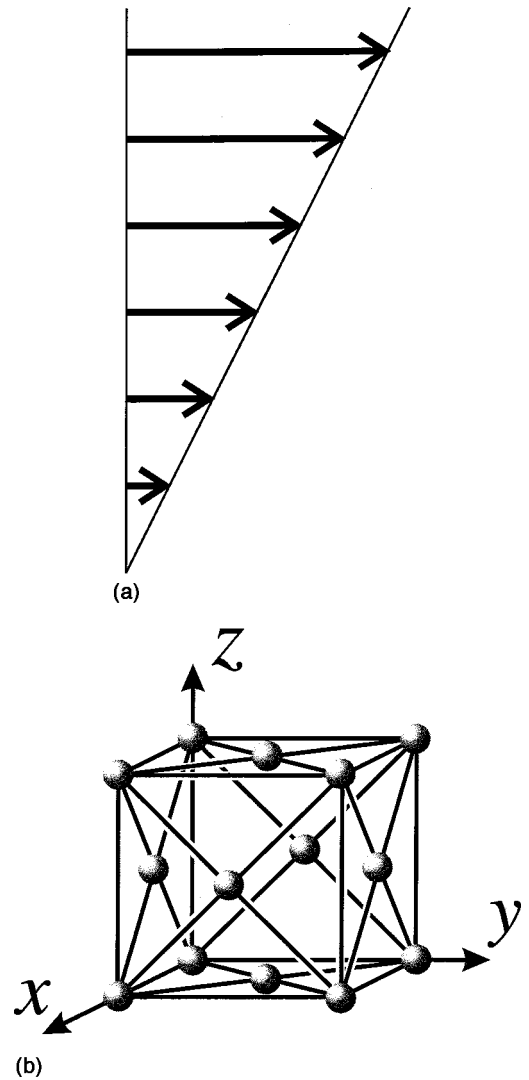


FIG. 16. fcc array of spheres (b) subject to a Couette flow in the yOz plane, as depicted in (a).

numerical simulation schemes, such as, e.g., the method of Stokesian dynamics [67,59]. The main ingredient for the evaluation of various structures is represented by lattice sums that can be efficiently computed using the method expounded in article I. The use of such a method is advocated, as it appears that neglect thereof has unnecessarily affected the calculations of Nunan and Keller in an adverse way.

The effective viscosity has been examined for simple tetragonal (st) lattices and the results for various structures of the st type can be qualitatively understood on the basis of the motion of the spheres in response to the ambient shear flow. The angular velocity of the spheres, relative to the shear flow, is shown to be nonzero for certain orientations of the st lattice with respect to the shear flow, in contrast to what is known for cubic arrays (see Ref. [36]). Finite viscosities are found in most cases where particle surfaces are in contact, where, for instance, the particles are allowed to perform a smooth rolling motion. The only example where the viscosity diverges for a st structure, or equally any other Bravais lattice, is for the case of close packing. The same is expected to hold for random hard-sphere suspensions. Our viscosity results for st lattices have been compared to the experimental data for an ordered suspension of hard spheres in an oscil-

lating shear flow, as reported by Gondret and Petit [66]. In Ref. [21] the experimental results were found to be described rather well by the known results for a sc lattice, although at moderate concentrations the structure observed in the experiments was characterized by parallel chains of close touching spheres. These chains were aligned in planes parallel to the direction of the shear flow and the chains were perpendicular to the plane of shear. On the basis of these observations Gondret and Petit proposed that the structure resembles an arrangement that we designated as st1. However, our numerical calculations for the shear viscosity for these st1 arrays show less correspondence with the experimental data than do the results for sc lattices. Another st lattice (st2) shows better agreement, but only in the range of high volume fractions. For increasing concentrations the experimental data show a distinctly different behavior when the volume fraction has passed that of sc close packing, and this is likely due to large changes in the microstructure. The numerical data for the previously proposed hexa2 structure [65] at high concentrations show a large discrepancy with the measurements over the complete range of volume fractions, while the curves for bct1 and bcc lattices also reveal a very different concentration dependence. However, the results for bct1 and bcc are seen to compare reasonably well for some of the higher concentrations, and this correspondence is better than was observed for all other structures that were considered (results for these other structures are not presented in this article),

with the exception of the fcc, lattice for which results are comparable with those for bct1. On the basis of our findings it is proposed that the suspension microstructure in the experiments by Gondret and Petit changes from a st type of arrangement to a bct- or fcc-like arrangement when the volume fraction is raised above that of sc close packing. This proposition may be decided by experimental verification. We are looking forward to further experiments on samples that contain a large number of particle layers, thereby reducing the effect of the solid walls on the apparent viscosity. In addition, it would be worthwhile to visualize the ordered suspension also at the highest possible concentrations, and in all three directions, so as to verify the existence of the st2-like structures that are suggested by our computations for $0.3 \leq \phi \leq 0.5$ and the arrangements of type bct or fcc at even higher volume fractions. It should be possible to examine the viscosity for colloidal crystals of finite thickness by a modification of the principal set of linear equations from which the components of the grand mobility matrix can be solved. Disordered structures can be treated by application of the quasi- N -particle approach that was formulated for colloidal crystals that are infinite in all three directions. Despite the fact that all computations presented in this article are for perfect lattices (with $N=1$) the results are found to describe the empirical data rather well, and it is expected, therefore, that this will stimulate further experimental investigation.

-
- [1] S. I. Henderson and W. van Meegen, *Phys. Rev. Lett.* **80**, 877 (1998).
- [2] P. P. J. M. Schram and S. A. Trigger, *Contrib. Plasma Phys.* **37**, 251 (1997).
- [3] A. E. Larsen and D. G. Grier, *Phys. Rev. Lett.* **76**, 3862 (1996).
- [4] A. Imhof and J. K. G. Dhont, *Phys. Rev. Lett.* **75**, 1662 (1998).
- [5] C. A. Murray, W. O. Sprenger, and R. A. Wenk, *Phys. Rev. B* **42**, 688 (1990).
- [6] M. Hoppenbrouwers and W. van de Water, *Phys. Rev. Lett.* **80**, 3871 (1998).
- [7] M. Hoppenbrouwers, Ph.D. thesis, Technische Universiteit Eindhoven, 1998.
- [8] P. P. J. M. Schram and S. A. Trigger, *Physica B* **228**, 91 (1996).
- [9] H. J. H. Clercx and P. P. J. M. Schram, *Phys. Rev. A* **46**, 1942 (1992).
- [10] J. Derksen and W. van de Water, *Phys. Rev. A* **45**, 5660 (1992).
- [11] A. J. Hurd, N. A. Clark, R. C. Mockler, and W. J. O'Sullivan, *J. Fluid Mech.* **153**, 401 (1985).
- [12] A. J. Hurd, N. A. Clark, R. C. Mockler, and W. J. O'Sullivan, *Phys. Rev. A* **26**, 2869 (1982).
- [13] M. A. Rutgers, J.-Z. Xue, E. Herbolzheimer, W. B. Russel, and P. M. Chaikin, *Phys. Rev. E* **51**, 4674 (1995).
- [14] R. Lahiri and S. Ramaswamy, *Phys. Rev. Lett.* **79**, 1150 (1997).
- [15] V. Yannopoulos, N. Stefanou, and A. Modinos, *J. Phys.: Condens. Matter* **9**, 10261 (1997).
- [16] D. Mei, H. Liu, B. Cheng, Z. Li, and D. Zhang, *Phys. Rev. B* **58**, 35 (1998).
- [17] R. Sprik and G. H. Wegdam, *Solid State Commun.* **106**, 77 (1998).
- [18] M. Parthasarathy and D. J. Klingenberg, *Mater. Sci. Eng., R.* **17**, 57 (1996).
- [19] A. T. Skjeltorp, *J. Appl. Phys.* **55**, 2587 (1984).
- [20] J. Liu, E. M. Lawrence, A. Wu, M. L. Ivey, G. A. Flores, K. Javier, J. Bibette, and J. Richard, *Phys. Rev. Lett.* **74**, 2828 (1995).
- [21] P. Gondret and L. Petit, *Phys. Fluids* **8**, 2284 (1996).
- [22] L. Petit and B. Noetinger, *Rheol. Acta* **27**, 437 (1988).
- [23] E. A. Allahyarov, L. I. Podlubny, P. P. J. M. Schram, and S. A. Trigger, *Physica A* **220**, 349 (1995).
- [24] B. U. Felderhof and R. B. Jones, *Z. Phys. B: Condens. Matter* **64**, 393 (1986).
- [25] P. Pieranski, *Contemp. Phys.* **24**, 25 (1983).
- [26] J. M. A. Hofman, H. J. H. Clercx, and P. P. J. M. Schram, *Physica A* **268**, 326 (1999).
- [27] H. J. H. Clercx and P. P. J. M. Schram, *Physica A* **174**, 293 (1991).
- [28] H. J. H. Clercx and P. P. J. M. Schram, *J. Chem. Phys.* **96**, 3137 (1992).
- [29] H. J. H. Clercx, Ph.D. thesis, Technische Universiteit Eindhoven, 1991.
- [30] J. Happel and H. Brenner, *Low Reynolds Number Hydrodynamics* (Prentice-Hall, London, 1965).
- [31] S. Kim and S. J. Karrila, *Microhydrodynamics: Principles and Selected Applications* (Butterworth-Heinemann, London, 1991).
- [32] G. K. Batchelor, *J. Fluid Mech.* **83**, 97 (1977).
- [33] G. K. Batchelor, *J. Fluid Mech.* **41**, 545 (1970).

- [34] R. Kapral and D. Bedeaux, *Physica A* **91**, 590 (1978).
- [35] M. Mooney, *J. Colloid Sci.* **6**, 162 (1951).
- [36] K. C. Nunan and J. B. Keller, *J. Fluid Mech.* **142**, 269 (1984).
- [37] H. J. H. Clercx and P. P. J. M. Schram, *Phys. Rev. A* **45**, 860 (1992).
- [38] E. J. Hinch, *J. Fluid Mech.* **83**, 695 (1977).
- [39] By definition the angular velocity $\boldsymbol{\omega}_a$ is half the vorticity, that is, $\boldsymbol{\omega}_a = (1/2)\nabla \times \mathbf{v}_a(\mathbf{r})$. According to convention the dot product in Eq. (2.1) is a contraction with respect to the *second* Cartesian index of \mathbf{g}_a , that is, $(\mathbf{g}_a \cdot \mathbf{r})_i = (\mathbf{g}_a)_{ij} r_j$.
- [40] Here pressure is understood to be the *excess* pressure that results after subtraction of *hydrostatic* pressure induced by some conservative force, e.g., gravity. This excess pressure is therefore the pressure change due to dynamic effects.
- [41] R. Schmitz and B. U. Felderhof, *Physica A* **113**, 90 (1982).
- [42] J. M. Normand, *A Lie Group: Rotations in Quantum Mechanics* (North-Holland, Amsterdam, 1980), pp. 459–473.
- [43] J. M. A. Hofman, Ph.D. thesis, Technische Universiteit Eindhoven, 1999.
- [44] To be precise, the coefficients $B_{2m}^{n\pm}$ can also be expressed in terms of the coefficients that determine the forces, torques, and stresslets, viz., $B_{1m}^{n\pm}$, $C_{1m}^{n\pm}$, and $C_{2m}^{n\pm}$.
- [45] J. M. Peterson and M. Fixman, *J. Chem. Phys.* **39**, 2516 (1963).
- [46] G. K. Batchelor and J. T. Green, *J. Fluid Mech.* **56**, 401 (1972).
- [47] B. U. Felderhof, *Physica A* **159**, 1 (1989).
- [48] M. Zuzovsky, P. M. Adler, and H. Brenner, *Phys. Fluids* **26**, 1714 (1983).
- [49] In the fluid region \mathcal{V}_f the velocity field $\mathbf{v}(\mathbf{r})$ in Eq. (5.4) represents the local fluid speed distribution, as before, while inside a particle, i.e., for $\mathbf{r} \in \mathcal{V}_p$, $\mathbf{v}(\mathbf{r})$ is conceived to be the local speed corresponding to the motion of the particle. It should be noted that because of the rigidity of the particles the subdomain \mathcal{V}_p does not contribute to the second integral in Eq. (5.4), but for the purposes at hand it is found convenient to retain the integral in its present form.
- [50] Roman indices i, j, k, l have been used here, instead of the greek indices $\alpha, \beta, \gamma, \delta$ in Eq. (5.13), in order to avoid confusion with the scalars α and β in Eq. (6.1).
- [51] Following conventional nomenclature the principal axes of a shear flow are defined as the lines in the directions of the eigenvectors of the (symmetrical) rate of strain tensor \mathbf{g}_a .
- [52] M. Zuzovsky, Ph.D. thesis, Carnegie-Mellon University, 1976.
- [53] H. Hasimoto, *J. Fluid Mech.* **5**, 317 (1959).
- [54] D. Bedeaux, R. Kapral, and P. Mazur, *Physica A* **88**, 88 (1977).
- [55] A. A. Zick and G. M. Homsy, *J. Fluid Mech.* **115**, 13 (1982).
- [56] J. M. A. Hofman, H. J. H. Clercx, and P. P. J. M. Schram, *Physica A* **268**, 353 (1999).
- [57] A. J. C. Ladd, *Phys. Fluids* **88**, 5051 (1987).
- [58] P. Mazur and W. van Saarloos, *Physica A* **115**, 21 (1982).
- [59] J. F. Brady, R. J. Phillips, J. C. Lester, and G. Bossis, *J. Fluid Mech.* **195**, 257 (1988).
- [60] B. J. Ackerson, *J. Rheol.* **34**, 553 (1990).
- [61] J. Laven, W. H. Boersma, J. Kaldasch, and H. N. Stein, in *International Symposium on Advances in Structured and Heterogeneous Continua*, edited by D. Siginer and Y. Yanovsky (Allerton Press, Inc., Moscow, 1993), pp. 479–492.
- [62] M. Tomita and T. G. M. van de Ven, *J. Colloid Interface Sci.* **99**, 374 (1984).
- [63] R. Pätzold, *Rheol. Acta* **19**, 322 (1980).
- [64] The analysis used by Nunan and Keller, which allows for an explicit evaluation of the particles' angular velocity, cannot be straightforwardly applied to noncubic lattices as it relies greatly on cubic symmetries.
- [65] P. Gondret and L. Petit, *C. R. Acad. Sci., Ser. IIB: Mec., Phys., Chim., Astron.* **IIB**, 25 (1995).
- [66] P. Gondret and L. Petit (private communication).
- [67] J. F. Brady and G. Bossis, *Annu. Rev. Fluid Mech.* **20**, 111 (1988).